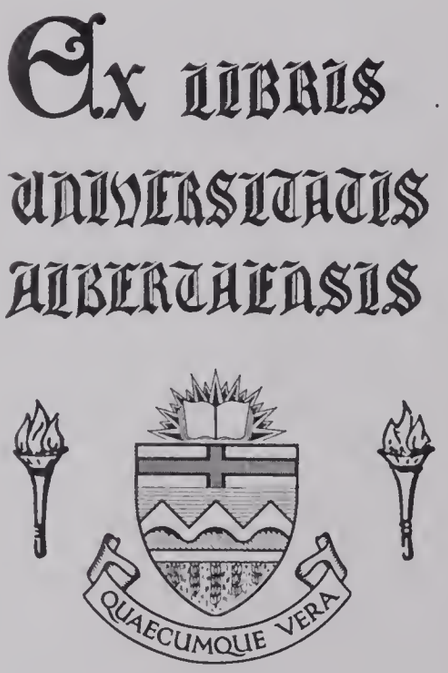

The University of Alberta
Printing Department
Edmonton, Alberta

UNIVERSITY OF ALBERTA
LIBRARY

Regulations Regarding Theses and Dissertations

Typescript copies of theses and dissertations for Master's and Doctor's degrees deposited in the University of Alberta Library, as the official Copy of the Faculty of Graduate Studies, may be consulted in the Reference Reading Room only.

A second copy is on deposit in the Department under whose supervision the work was done. Some Departments are willing to loan their copy to libraries, through the inter-library loan service of the University of Alberta Library.

These theses and dissertations are to be used only with due regard to the rights of the author. Written permission of the author and of the Department must be obtained through the University of Alberta Library when extended passages are copied. When permission has been granted, acknowledgement must appear in the published work.

This thesis or dissertation has been used in accordance with the above regulations by the persons listed below. The borrowing library is obligated to secure the signature of each user.

Please sign below:

Date	Signature	Institution

THE UNIVERSITY OF ALBERTA

A STUDY OF TRANSIENT LINEAR GAS FLOW THROUGH POROUS MEDIA

BY

COURTNEY C. FORTEMS

A THESIS

SUBMITTED TO THE FACULTY OF GRADUATE STUDIES

IN PARTIAL FULFILMENT OF THE REQUIREMENTS FOR THE

DEGREE OF MASTER OF SCIENCE

IN

PETROLEUM ENGINEERING

FACULTY OF ENGINEERING

DEPARTMENT OF CHEMICAL AND PETROLEUM ENGINEERING

EDMONTON, ALBERTA

MARCH, 1968

UNIVERSITY OF ALBERTA

FACULTY OF GRADUATE STUDIES

The undersigned certify that they have read, and recommend to the Faculty of Graduate Studies for acceptance a thesis entitled A STUDY OF TRANSIENT LINEAR GAS FLOW THROUGH POROUS MEDIA submitted by Courtney C. Fortems in partial fulfilment of the requirements for the degree of Master of Science in Petroleum Engineering.

ACKNOWLEDGEMENT

The author wishes to express his gratitude to Dr. D. L. Flock, Professor, Department of Chemical and Petroleum Engineering, University of Alberta, for his encouragement, guidance and supervision during the course of this investigation.

Furthermore, the financial assistance which enabled this study to be completed was gratefully received from the University of Alberta and the Alberta Oil and Gas Conservation Board.

Finally, the author wishes to express his appreciation to his wife, Ruthie, for her encouragement and assistance in completing this thesis, and Miss Marilyn Hornby for typing the manuscript.

ABSTRACT

Few previous investigators have attempted to experimentally study unsteady state flow of gas through porous media. Instead, they have predicted transient behaviour by various approximations to the non-linear partial differential equation describing such flow.

In the course of this investigation, the transient behaviour was measured directly by flowing nitrogen through relatively long full-sized core samples. The experimental results were scrutinized and compared with numerical solutions to a mathematical model. The boundary conditions simulated were:

1. Constant terminal pressure with constant pressure at the external boundary.
2. Constant terminal pressure with a sealed external boundary.

The results obtained indicate the shortcomings of certain types of flow systems, the desirability of long flow systems and the behaviour of pressure transients in both homogeneous and heterogeneous systems. Furthermore, the investigation illustrates the approximation to experimental results obtained by means of the mathematical model.

TABLE OF CONTENTS

LIST OF FIGURES

INTRODUCTION

Petroleum industry studies involving unsteady state or transient flow generally are concerned with analysis of well tests or water influx. The well tests include drawdown, buildup, interference and back-pressure tests which can be utilized to evaluate such quantitative information about a well and reservoir as wellbore damage, effective permeability within the drainage radius, static reservoir pressure, distances to boundaries, inter-well communication, reservoir size and capabilities. These evaluations are simply applications of solutions of modified forms of the continuity equation. A very general form of the continuity equation is given below.

$$\nabla \cdot \left[\rho \vec{v}\right] = -\phi \frac{\partial \rho}{\partial t}$$

In the case of water influx, the aquifer response is related to the variations of the average boundary pressure by solutions to the continuity equation. Van Everdingen and Hurst [31] have solved this form of the continuity equation for influx and have presented the results in convenient tabular and graphical forms in terms of dimensionless quantities.

The objective of this study was to experimentally measure and examine unsteady state or transient gas flow in porous media.

In general terms this type of fluid flow can be described by the continuity equation. Substitution of an equation of motion and an equation of state into the continuity equation yields a form of the diffisivity equation utilized in this study. This form of the diffusivity equation describes isothermal, viscous flow of a real gas in a linear, horizontal system.

Darcy's law which was used as the equation of motion is limited to the viscous flow regime and does not account for slip and inertial energy losses. The seriousness of this simplification was given a cursory examination by comparing the numerical results obtained from a mathematical model and the experimental results. The model incorporates the variation of viscosity and compressibility with pressure and the variation of absolute permeability with position.

THEORY AND LITERATURE REVIEW

The movement of gas through porous media has been extensively investigated, and from these investigations three flow regions have been established for separate consideration: (a) molecular streaming, (b) viscous, and (c) turbulent flow.

Scheidegger [29] summarizes significant theoretical and experimental contributions in these vital regions. These early examinations deal with steady state flow primarily, wherein the pressure and fluid velocity at every point throughout the system adjust instantaneously to either a pressure or flow rate change in some other part of the system.

More recently, the unsteady state or transient flow of gas has been receiving considerable attention, especially in relation to back pressure testing and pressure build up analysis. Expansion of compressed reservoir fluids during production results in unsteady state flow. When a well is opened for flow, a pressure drop occurs at the wellbore causing fluid in the vicinity of the wellbore to expand and flow towards it. As a result of this fluid loss, the reservoir pressure more remote from the wellbore declines, permitting the fluid there to expand and to flow towards the well. Consequently the drainage area continues to expand, and the

velocity and pressure are continuously changing at all points. Hence, in an elemental volume of porous media, the flow rate into the media is not the same as that out of the media.

An equation which properly describes transient flow must firstly involve a material balance:

$$\left[\begin{array}{c}\text{Amount of}\\ \text{Mass Input}\end{array}\right] - \left[\begin{array}{c}\text{Amount of}\\ \text{Mass Output}\end{array}\right] = \left[\begin{array}{c}\text{Increase of Mass}\\ \text{Within the Region}\end{array}\right]$$

Based on the conservation of mass for isothermal fluid flow through a porous medium, the material balance takes the form of the well-known continuity equation:

$$\nabla \cdot \left[\rho \vec{v}\right] = - \phi \frac{\partial \rho}{\partial t} \qquad (1)$$

The vector in Equation 1, which represents the volumetric rate of flow per unit cross-sectional area, can be expressed by Darcy's Law if the flow is viscous:

$$\vec{v} = - \frac{k(p)\,\rho}{\mu(p)} \nabla \Phi \qquad (2)$$

Hubbert[17] has studied Darcy's Law and its implications and has indicated that:

$$\Phi = \int_{p_o}^{p} \frac{dp}{\rho} + gZ \qquad (3)$$

Generally gravitational effects are ignored, and Darcy's Law becomes:

$$\vec{v} = - \frac{k(p) \nabla p}{u(p)} \qquad (4)$$

At high velocities, Darcy's Law no longer expresses the relationship between the flow rate and the pressure gradient, but must be replaced by an equation incorporating a quadratic velocity term:

$$D\vec{v} |v| + \vec{v} = - \frac{k(p)}{u(p)} \nabla p \qquad (5)$$

However, assuming viscous flow, the combination of the continuity equation (Equation 1) and Darcy's Law (Equation 4) yields a differential equation describing fluid flow in a porous medium.

$$\nabla \cdot \left[\rho \frac{k(p)}{u(p)} \nabla p \right] = \phi \frac{\partial \rho}{\partial t} \qquad (6)$$

The final form of the equation which adequately describes unsteady state flow through porous media depends on the fluid and the equation of state. For real gases:

$$\rho_g = \frac{M}{RT} \frac{p}{z(p)} \qquad (7)$$

Eliminating density (ρ) from Equation 6 and assuming isothermal flow will yield:

$$\nabla \cdot \left[\frac{k(p)}{u_g(p)\, z(p)} \, p \nabla p \right] = \phi \, \frac{\partial}{\partial t} \left[\frac{p}{z(p)} \right] \tag{8}$$

Equation 8 with necessary boundary and initial conditions along with appropriate correlations relating permeability, viscosity, and compressibility factor to pressure, will mathematically describe the flow of gas through a porous medium. The proposed experimental study involves no more than analysing the pressure behaviour as a function of both position and time and comparing this with numerical solutions to Eq. 8.

A search through the literature revealed that the experimental examination of unsteady state gas flow is very limited. Therefore, despite this being primarily an experimental study, a review of the theoretical investigations related to this type of flow was undertaken to better understand the implications of Equation (8) and its associated assumptions. Most of the theoretical solutions involved the simplifying assumptions of constant (a) permeability, (b) viscosity and (c) compressibility factor, which reduces Equation (8) to:

$$\nabla \cdot \left[p \nabla p \right] = \frac{\phi \mu}{k} \, \frac{\partial p}{\partial t} \tag{9}$$

The methods included pseudo-steady state, analytical, graphical, numerical and analogue solutions. A review of graphical and analogue solutions will not be presented here, but can be found in Katz et al [18]. One of the earliest attempts to solve Equation (9) was made by Heatherington, MacRoberts and Huntington[15]. Realizing that nearly all phenomena of practical interest in gas production involved unsteady state flow, and that the pertinent equation was not mathematically reducible to simple expressions void of infinite series, Heatherington et al proposed an approximate solution based upon "infinite series of steady states". With time no longer an independent variable, the equation was solved by simple, explicit integration. The authors were able to conclude from a comparison of experimental and theoretical data that the general back-pressure equation was reasonably accurate, provided the initial transient period was not too long.

Muskat [24] similarly obtained solutions to Equation (9) by assuming a "succession of steady states". This implies that the velocity of the propogation of disturbances in a porous medium is infinite, while the mass fluid content variation of the system is negligible compared to the steady state flux through the system.

However, as indicated by Muskat, these two assumptions could be most inaccurate if the system were very large or where abnormally high compressibilities were encountered. He proceeds to illustrate by example how an oil system containing as little as 4.5 per cent free gas would have sufficiently high compressibility to make the application of "succession of steady states" invalid.

Utilizing the steady state formula for radial gas flow, Aronofsky and Jenkins [3] approximated the transient solution to Equation (9) by suitably defining an effective drainage radius. Furthermore, these authors were able to conclude that the solutions for the liquid flow case could be used to generate approximate solutions for the constant rate of production of ideal gases. Extending this approach, Al-Hassainy, Ramey and Crawford [1] approximated Equation (8) by introducing a variable change applicable to the flow of real gases through porous media. This change was used as a pseudo-pressure consisting of pressure as well as the pressure dependent quantities of viscosity and compressibility factor. The final form of the diffusivity equation simply has pressure squared replaced by the pseudo-pressure term.

A summary of the more significant analytical solutions is presented by Katz et al [18] in tabular and graphical form for both linear and radial flow. The mathematical derivation for linear flow was obtained from heat flow studies by Churchill[9], while the radial flow solutions were developed by Van Everdingen and Hurst[31]. Roberts [28] obtained an approximate analytical solution to the one dimensional form of Equation (9). He employed a stepwise forward integration with respect to time to solve a linearized form of the partial differential equation. By comparing the results to those obtained when assuming the gas obeyed the linear heat conduction equation, he showed that the non-linearity reduced the rate of pressure decline. Kidder [20], applying perturbation techniques and utilizing the well-known Boltzmann transformation, presented an analytical solution for gas flow in a semi-infinite porous medium.

With the advent of digital computers, numerical solutions using both finite difference equations and computing techniques have become very popular. Aronofsky and Jenkins [2] obtained solutions to the one dimensional form of Equation (9) by employing a forward difference explicit (FDE) approximation modified with respect to time to insure stability. They observed from finite

tube studies that the non-linear character of the equation caused the solution to approach steady state more rapidly for the larger ratios of initial pressure to constant terminal pressure. Similarly, Bruce, Peaceman, Rachford and Rice [6], utilizing FDE, obtained solutions for linear flow. However, they also determined by an implicit technique, the solutions for linear and radial flow.

The linear and radial forms of Equation (8), with permeability constant, were solved by Aronsfsky and Ferris [4] and by Aronsfsky and Porter [5] respectively. The radial consideration was modified to insure stability by assuming a steady state core around the wellbore. These authors observed that the influence of varying gas properties had a significant effect on the time dependency of the pressure.

Quon, Dranchuk, Allada and Leung [25, 26] discussed five numerical techniques for handling Equation (8) in a two dimensional system. These techniques are: (a) forward difference explicit (FDE), (b) backward difference implicit (BDI), (c) Crank-Nicholson implicit (CNI), (d) alternating - direction explicit procedure (ADEP) and (e) alternating-direction implicit procedure (ADIP). Quon et al concluded ADEP offers computer efficiency over the implicit procedures and has a stability advantage over FDE.

Carter[8] examined three methods of solving Equation (8) in a two dimensional model and observed that implicit procedures of the Saul'ev type are stable for practical time step sizes. Furthermore from a computing time viewpoint, these procedures are more desirable than the explicit techniques.

Eilerts[13] presents solutions to Equation (8) for flow of gas condensate fluids in linear and radial systems. Viscosity and compressibility are treated as functions of pressure while permeability is a function of pressure and position. The resulting partial differential equation is written in the form of finite differences and solved by available explicit and implicit procedures.

This study involves a comparison of experimental unsteady-state flow data with that predicted by a one-dimensional mathematical model. Since it was desirable that the model incorporate variability of viscosity and compressibility with pressure and the variability of permeability with distance, the diffusivity equation (Eq. 8) was modified to give:

$$\frac{\partial}{\partial x}\left[\frac{K(x)\,p}{\mu_g(p)\;z(p)}\;\frac{\partial p}{\partial x}\right] = \phi\,\frac{\partial}{\partial t}\left[\frac{p}{z(p)}\right] \qquad (10)$$

Variation of viscosity and compressibility with pressure was provided by correlations found in the literature [16, 19] while position variation of permeability was obtained from steady state calculations. Furthermore the equation was linearized with respect to p^2 by introducing a mean pressure:

$$\frac{\partial}{\partial x}\left[\frac{K(x)}{\mu(p)\, z(p)}\frac{\partial p^2}{\partial x}\right] = \frac{\phi}{\bar{p}}\frac{\partial}{\partial t}\left[\frac{p^2}{z(p)}\right] \qquad (11)$$

Finally, specification of the initial and boundary conditions to be imposed for the constant terminal pressure case completes the model.

Constant Pressure at External Boundary

Initial Condition

$$p(x, 0) = p_i \qquad o \leq x \leq L$$

Boundary Conditions

$$p(o, t) = p_w \qquad t > o$$

$$p(L, t) = p_i \qquad t > o$$

Sealed External Boundary

Initial Condition

$$p(x, o) = p_i \qquad o \leq x \leq L$$

Boundary Conditions

$$p(o, t) = p_w \qquad t>o$$

$$\left.\frac{dp}{dx}\right|_{x=L} = o \qquad t>o$$

Crank-Nicholson finite difference equations as proposed by Eilerts [13] and the square root algorithm extended to non-symmetric matrices, were utilized in the solution to the diffusivity equation.

Appendix A presents the derivation of the PDE while Appendix B illustrates the details of the discretization of the finite difference equations which were solved on an IBM 360/67 digital computer. Details of the program are described and presented in Appendix C.

EXPERIMENTAL APPARATUS

In conjunction with the measurement of pressure transients, the experimental determination of the absolute permeability and porosity necessitated measurements of pressure, temperature and flow rate. To accomplish this a wide variety of equipment was required.

A porosimeter was constructed to facilitate pore volume measurement of the large, encased core samples. The essential components of this equipment as shown in Figure I are a calibrated Marsh gauge to measure the initial pressure of the system, an expansion chamber, a mercury manometer to measure the expanded pressure and a vacuum pump.

Figure II is a composite diagram of the experimental equipment used in procuring permeability and transient data. This is essentially the same experimental apparatus employed by Cachero[7] with a few modifications. These changes include (1) a Moore Nullmatic pressure regulator (2) a sixth transducer (3) one half inch O. D. flow line on the downstream side of the core. Constant boundary pressures were ensured by the first and third modifications while the second provided a check of pressure drop across the core as measured by the pressure gauges.

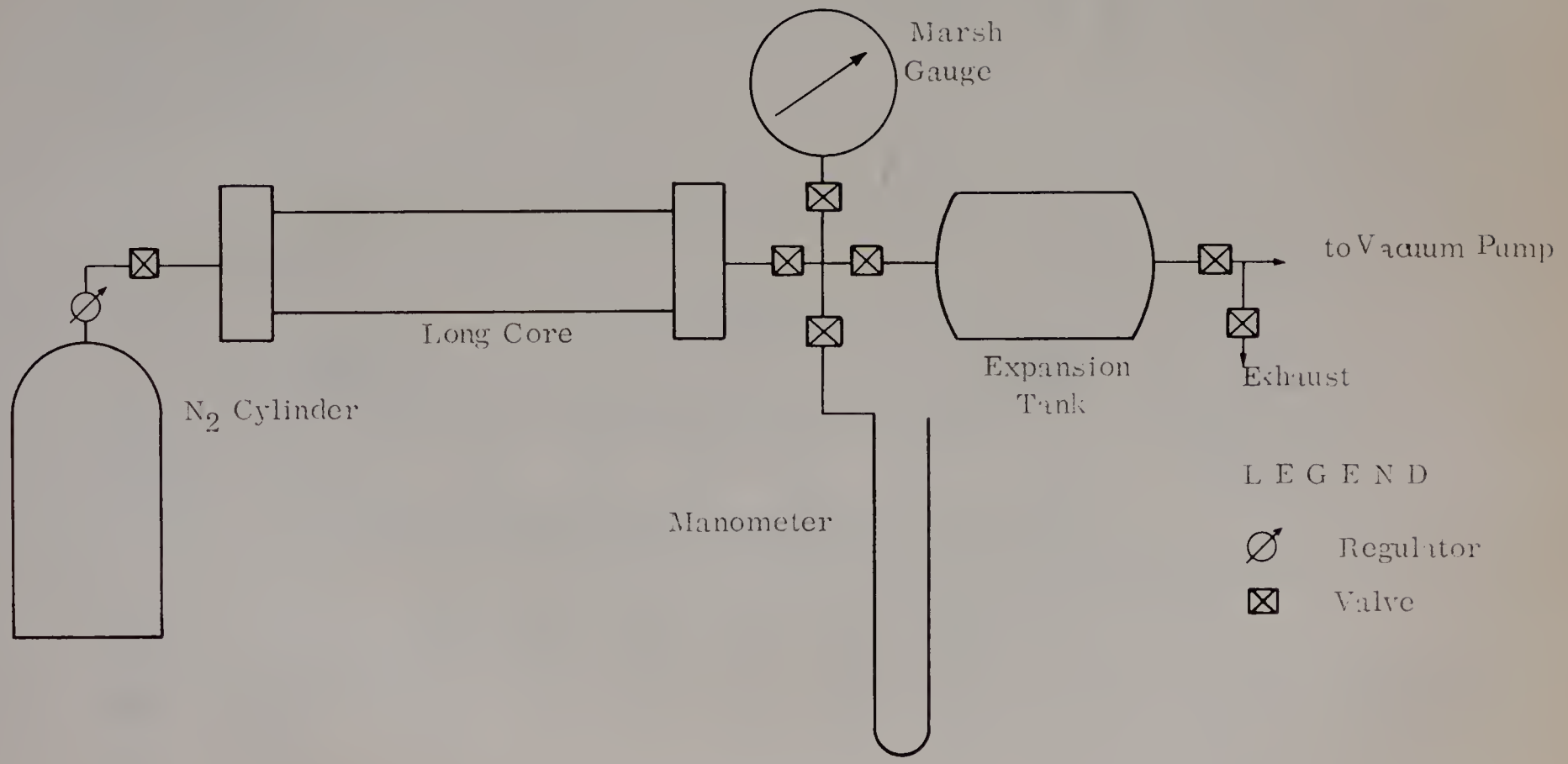

FIGURE 1

POROSIMETER

FIGURE 2

DIAGRAM OF EXPERIMENTAL APPARATUS

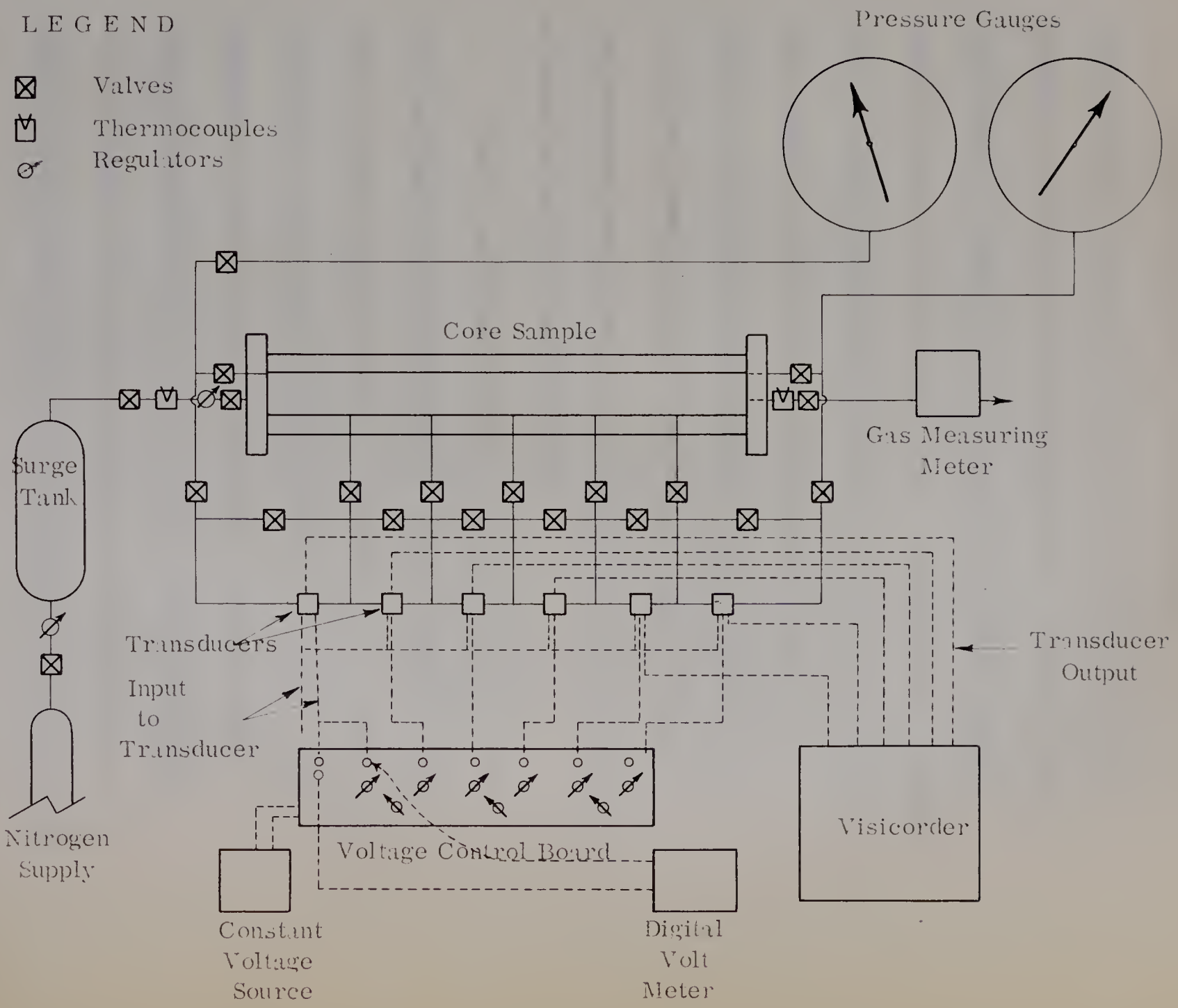

A cylinder charged with commercially pure nitrogen was equipped with a regulator to provide gas at a relatively constant pressure. Additional control was supplied by a pressure cylinder functioning as a surge tank and the nullmatic pressure regulator installed upstream from the core holder. Preceding this regulator and immediately downstream from the core holder were flowline iron-constantan thermocouples for temperature measurement. Bourdon tube pressure gauges tapped into each end plate of the core holder provided means of measuring pressure. Flow rate measurements were made by a three-range Vol-O-Flo meter and a Precision Instrument wet test meter.

Finally, the pressure distribution along the length of the core was obtained using calibrated high pressure Statham differential pressure transducers whose output voltage was continuously recorded by a multi-channel Honeywell 906 A visicorder. Input voltage to the transducers was provided by a constant voltage source and checked with a digital voltmeter. With the exception of the nitrogen cylinder, pressure gauges, and the flow meter, the apparatus was enclosed within a thermostatically controlled cabinet.

EXPERIMENTAL PROCEDURE

CORE MOUNTING AND CLEANING PROCEDURE

A berea sandstone model labelled Berea 1 in this study and a Series core were those prepared by Cachero. In addition to the aforementioned cores, full size Berea sandstone and limestone samples were selected for non-steady state study. These cores were sheared off at a desired length as described by Hamilton [14] in an attempt to avoid possible mechnical end effects. After being centered in casing by a mounting board and wedges, the cores were set using the identical technique and epoxy resin employed by Mackett [23]. These two cores plus the Berea 1 core were set in five and one-half inch casing. Thus the one set of end plates would serve all three cores. The Series core was mounted in four and one-half inch casing and was equipped with a set of screw-on end plates. All cores were tapped with five equally spaced taps drilled through the casing and epoxy to the core surface. The Berea 1 and Series core are illustrated in Figure 3.

The mounted cores were flushed with isoctane, chased by propane and dried with nitrogen prior to testing.

FIGURE 3

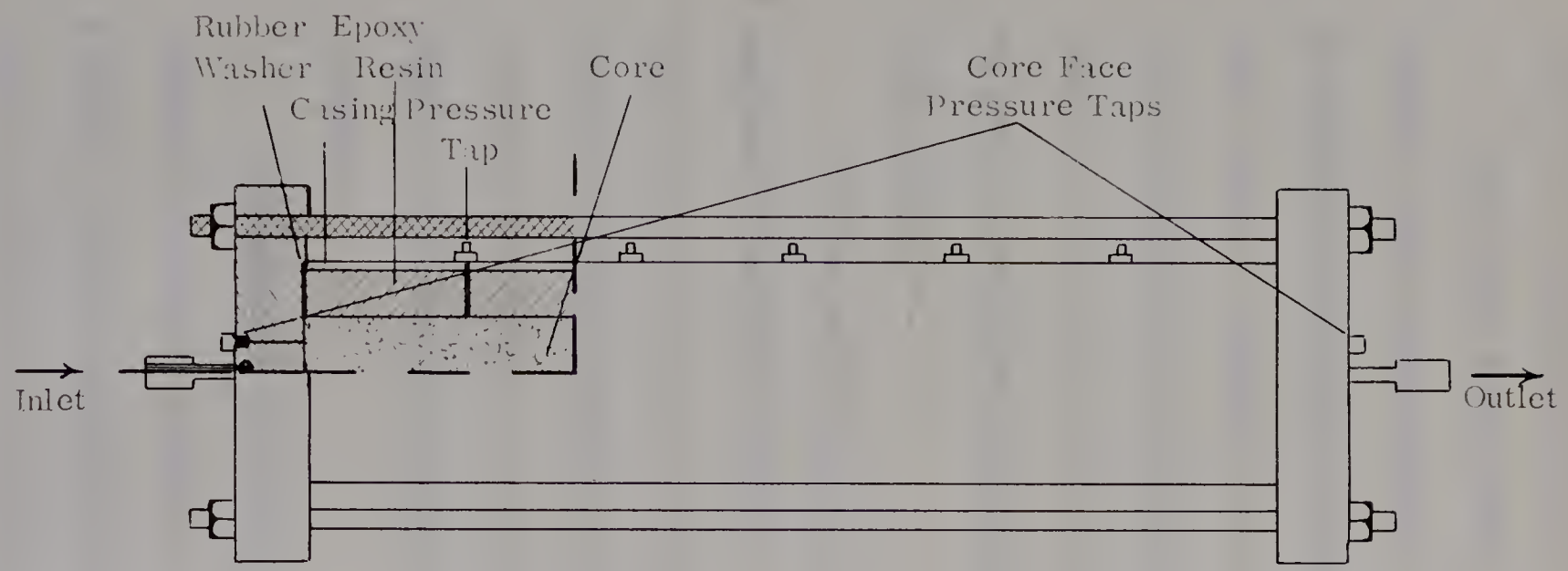

BEREA I CORE AND HOLDER

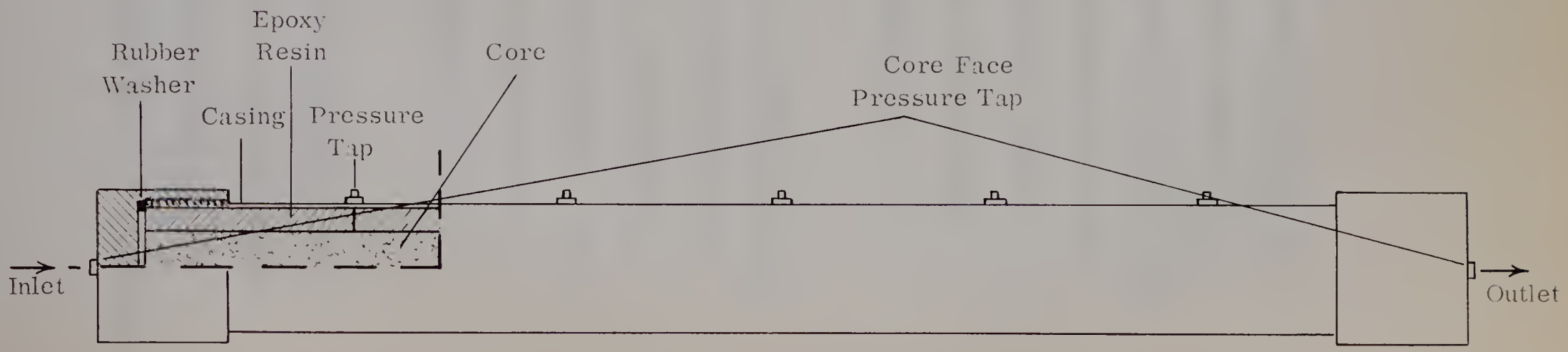

SERIES CORE AND HOLDER

EFFECTIVE POROSITY DETERMINATION

Bulk volume determination of the mounted cores was performed by direct measurement of diameter and length, while the gas expansion porosimeter provided the gross grain volume. Four trials, each at a different initial pressure ensured that the pore volume determination was not pressure dependent. That is, expansion of the casing and/or epoxy annulus while the system was pressurized did not significantly affect porosity.

FLOW TESTS

Flow data were obtained on all cores using the experimental equipment illustrated in Figure 2. Prior to testing, the system was checked under pressure for leaks using a soap solution and observing a possible decline in pressure gauge readings. During permeability flow tests the tranducers were isolated from the system to avoid excessive pressure differentials on any one transducer.

A permeability determining flow test commenced with the setting of the nullmatic pressure regulator at the desired upstream pressure. Periodic observation of the upstream and downstream pressure and the flow rate indicated when steady state flow conditions

had been attained and various observations could be recorded. At pressures in excess of the operating limits of the nullmatic regulator, it was removed with upstream pressures being subsequently controlled by the regulator on the nitrogen bottle.

Each experimental run included the following recordings (1) upstream core-face pressure, (2) downstream core-face pressure, (3) upstream thermocouple reading, (4) downstream thermocouple reading, (5) flow rate reading, (6) barometric pressure, and (7) room temperature reading.

The unsteady state flow tests were conducted using the same experimental setup; however, in this case the transducers were in communication with the pressure taps but isolated from each other.

It was desirable to examine two different boundary conditions. Firstly, constant terminal pressure with a constant pressure at the external boundary and secondly, constant terminal pressure with a sealed external boundary. The first boundary condition was simulated by closing the downstream toggle valve and adjusting the nullmatic pressure regulator to pressurize and provide the system with the desired initial pressure. Then, the visicorder's chart time and

speed were set and the downstream snap action valve was opened. Closure of the valve immediately upstream from the core prior to drawdown provided data for the second set of boundary conditions.

Typical experimental data recorded during each test immediately prior to the test were (1) visicorder time and speed setting, (2) upstream core-face pressure, (3) downstream core-face pressure, (4) upstream thermocouple reading, (5) downstream thermocouple reading, (6) barometric pressure, and (7) room temperature reading. Furthermore, the upstream core-face pressure was recorded at various times to provide a check and the upstream and downstream core-face pressures were again recorded once steady state conditions had been achieved.

Initially, flow rates at various times during each test were to be recorded; however, it was found that with the additional equipment downstream of the core-face, constant terminal pressure could not be achieved prior to the transients reaching the upstream core face.

PROCESSING OF EXPERIMENTAL RESULTS

POROSITY MEASUREMENTS

Table I was prepared from direct measurements and from evaluated porosimeter data.

TABLE 1

Core	Diameter (Inches)	Length (Inches)	Bulk Volume (Cu. In.)	Porosity (Fraction)
Berea 1	3.51	34.3	320.8	.208
Berea 1A	3.51	20.8	201.3	.196
Berea 2	3.51	21.4	209.7	.237
Limestone	3.51	21.5	203.1	.213
Series	1.997	54.0	169.1	.264

Cores Berea 1 and Berea 1A are the same test samples. The Berea 1 sample was that studied by Cachero but with three-eights of one inch fractured off each end to examine mechanical end effects. Berea 1A was the same sample with an additional six and one-half inches removed from each end.

STEADY STATE MEASUREMENTS

The liquid or absolute permeability of each core sample was initially determined by applying the appropriate form of Darcy's

law to test data in the viscous flow region and correcting for slippage as suggested by Klinkenberg[21]. A computer program eliminated most of the manual calculations.

Upon examining the back-pressure plots corrected for slip as per Dranchuk and Kolada[12], it was evident that some viscous inertial data was being included in the original permeability determinations for the Limestone sample. Furthermore, flow test data for the Series core were almost entirely in the visco-inertial region. The former problem was corrected by eliminating the visco-inertial data from the calculation while the latter was resolved by determining permeability by the technique proposed by Dranchuk and Sadiq[11]. Following is a summary of the permeability data.

TABLE 2

Core	Liquid Permeability (MDS)
Berea 1	4.74
Berea 1A	10.33
Berea 2	550.4
Limestone	6.20
Series	606.0

The scattering of the steady state data which was observed at low flow rates was also observed by Mackett[23] in an earlier study and attributed to inaccuracies of the Vol-O-Flo meter.

UNSTEADY STATE MEASUREMENTS

A number of transient flow tests were performed on each core. The visicorder readings, which represent pressure differentials across individual sections of a core, were combined with the upstream and downstream core-face pressure to yield pressure profiles for varying cumulative times.

During the early flow period, prior to the transient reaching the external boundary, the differential pressure readings were subtracted from the known upstream pressure to yield the downstream pressure and provide a check of that pressure. However on occasion, a discrepancy was encountered and in those incidents the deviation was distributed proportionally over all pressure differentials.

At later times when the transient had attained the upstream end of the core and the downstream core-face had stabilized, profiles were obtained by adding differentials to this stabilized pressure. Any discrepancies resulting from the check of the upstream pressure were treated identically to those encountered at early flow times.

Negative pressure differentials were observed during the processing of data for the Berea 2 and Limestone samples. Such differentials were treated as zero differentials and any discrepancy arising from the pressure check were proportionally distributed across the pressure profile. These occurrences are explained in the following section.

Unsteady state flow tests on each sample involving the boundary conditions of constant terminal pressure with constant pressure at the external boundary were continued until steady state conditions had been attained. The resulting steady state pressure profile was utilized to calculate the permeability of each section of the sample. Table 3 lists the permeability distribution of each sample. The permeabilities are in millidarcies.

TABLE 3

Permeability of Sections

	1	2	3	4	5	6
Berea 1	1.46	42.1	41.2	22.5	14.4	1.30
Berea 1A	2.61	8.05	234.	234.	15.0	9.80
Berea 2	653.	627.	674.	655.	476.	378.
Limestone	10.8	14.8	283.	282.	2.39	2.37
Series	473.	535.	533.	662.	652.	767.

DISCUSSION OF RESULTS

EXPERIMENTAL RESULTS

Experimental unsteady state flow tests were conducted on the five core samples for the following two different sets of boundary conditions.

1. Constant terminal pressure case with constant pressure at the external boundary.
2. Constant terminal pressure case with a sealed external boundary.

A typical example of results obtained from such flow tests is presented in Figure 4 for the limestone sample. The ordinate represents the pressure term $p(x, t)$, which is a function of distance x and time t while the abscissa is the dimensionless distance x/L where L is the overall length of the system.

The pressure distribution in Figure 4 corresponding to $t = 0.1$ minutes exhibited the pressure drawdown occurring at the downstream core-face upon opening the toggle valve to achieve constant terminal pressure at this end of the system. During this period the production originated from the region in the immediate vicinity of the producing face. Furthermore, as a result of this fluid loss through production additional pressure

FIGURE 4
PRESSURE DISTRIBUTION
LIMESTONE: CONSTANT TERMINAL PRESSURE WITH
CONSTANT PRESSURE AT EXTERNAL BOUNDARY

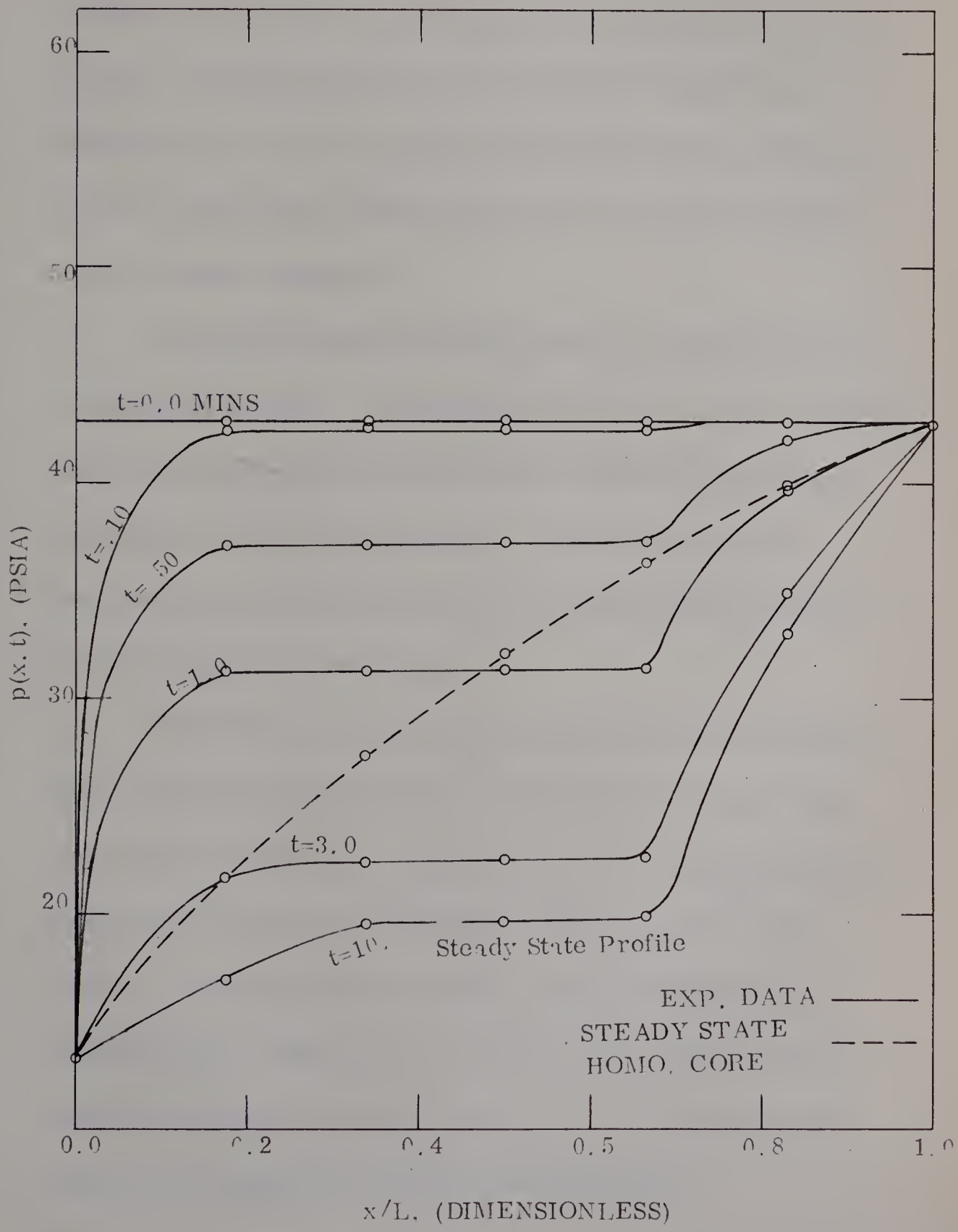

declines occurred more remote from the producing end thus permitting the fluid there to expand and flow towards this end of the system. In this way the pressure disturbance originating at the downstream core-face propagated through the system which had behaved as if it were infinite as long as the disturbance had not reached a finite boundary.

Finite behaviour commenced when the transient reached the external boundary. The distribution at t=0.5 minutes illustrates the first trace of finite behaviour with constant pressure being maintained at the external boundary. Furthermore with the commencement of finite behaviour, the heterogeneous nature of the core sample became evident.

The Limestone sample had a low permeability section on the upstream end resulting in the comparatively large pressure drop observed from x/L = 0.664 to x/L = 1.0. This tight section substantially reduced the flow of gas to the more permeable sections, consequently these sections depleted almost as if a sealed boundary exists at x/L = 0.664. Upon reaching steady state the depletion was almost complete in the higher capacity sections as exhibited by the pressure distribution.

The extent of the depletion resulting from the heterogeneous nature of the sample was illustrated by comparing the mean pressures of the steady state profiles of the experimental data and that of a homogeneous system. Had the core been homogeneous, the steady state pressure distribution would have been identical to the theoretical one depicted by the dashed line on Figure 4 which resulted in a mean pressure of 30.3 psia. The mean pressure associated with the experimental steady state profile was 23.6 psia.

Application of the second set of boundary conditions to the limestone core yielded results as presented in Figure 5. Initially the pressure distributions were identical to those of the first set of boundary conditions; however, upon reaching the external boundary they were observed to decline more rapidly. This behaviour can be attributed to the lack of flow across the external boundary. Again, the tight section on the upstream end of the sample was apparent.

A peculiar problem arising while conducting unsteady state flow tests on the Indiana limestone sample was the occurrence of negative pressure differentials for both sets of boundary conditions. One possible explanation would be a localized pressure

FIGURE 5
PRESSURE DISTRIBUTION
LIMESTONE: CONSTANT TERMINAL PRESSURE WITH
SEALED EXTERNAL BOUNDARY

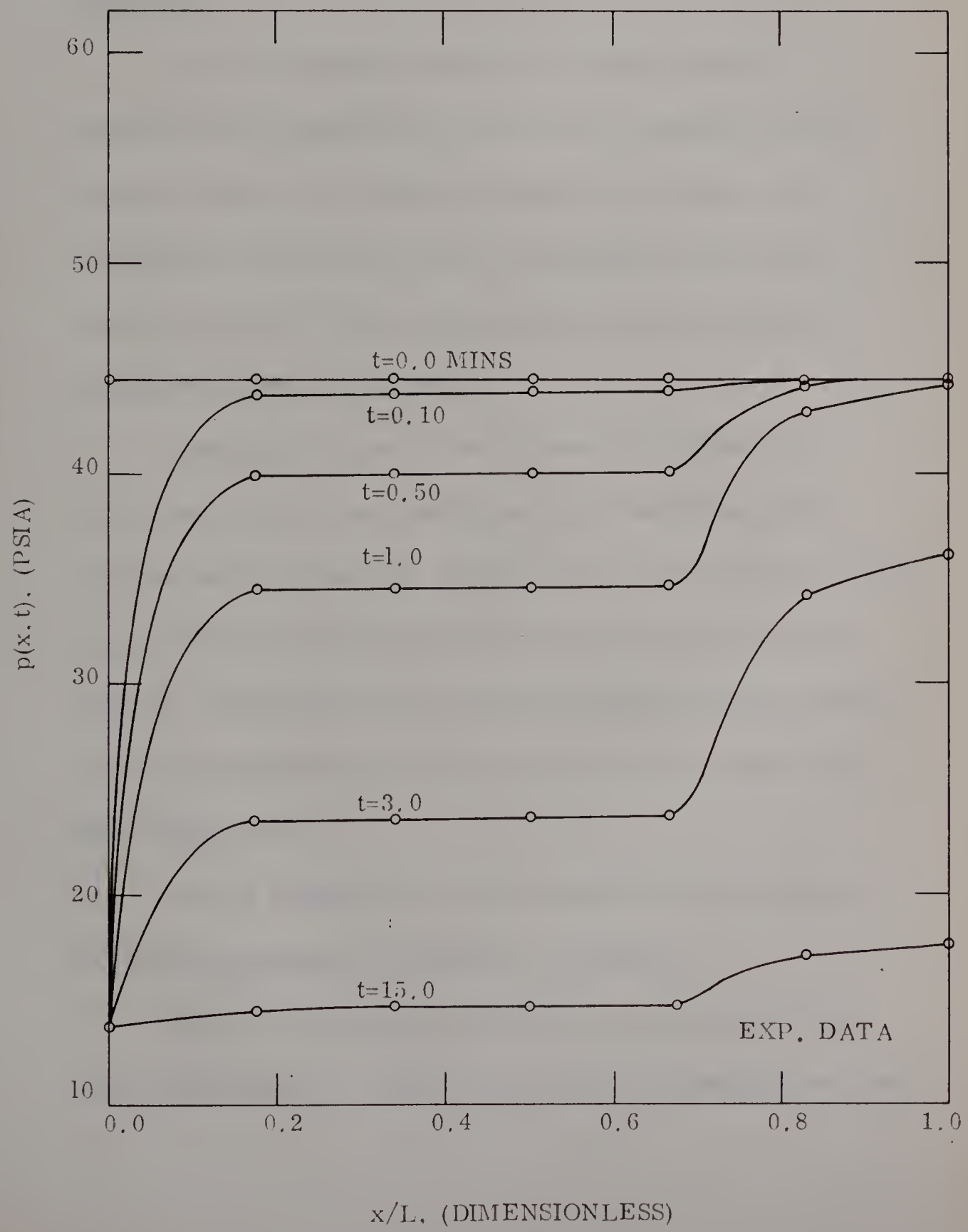

expansion in the immediate vicinity of the affected pressure taps resulting in an decreased fluid velocity and the resultant negative differential.

A more reasonable explanation might be a severe reduction of the transmissibility of the pore channels in the immediate vicinity of the effected pressure taps because of the mechanical drilling of the taps. This damaged surface would delay the response of the corresponding transducer and result in negative pressure differentials.

Assuming the latter to be the case, the affected taps were scraped with a sharp instrument and cleaned out, but no improvement was observed. Perhaps if the core had been reversed or equipment modifications made this problem might have been resolved. Modifications could include changing to static pressure recording transducers or drilling more than one pressure tap at each length location.

Results of unsteady flow tests conducted on the other core samples are graphically illustrated in Appendix D.

Figure 6 illustrates the heterogeneous behaviour of the Berea 1 core sample. Cachero in an earlier investigation believed

FIGURE 6
PRESSURE DISTRIBUTION
BEREA 1: CONSTANT TERMINAL PRESSURE WITH
CONSTANT PRESSURE AT EXTERNAL BOUNDARY

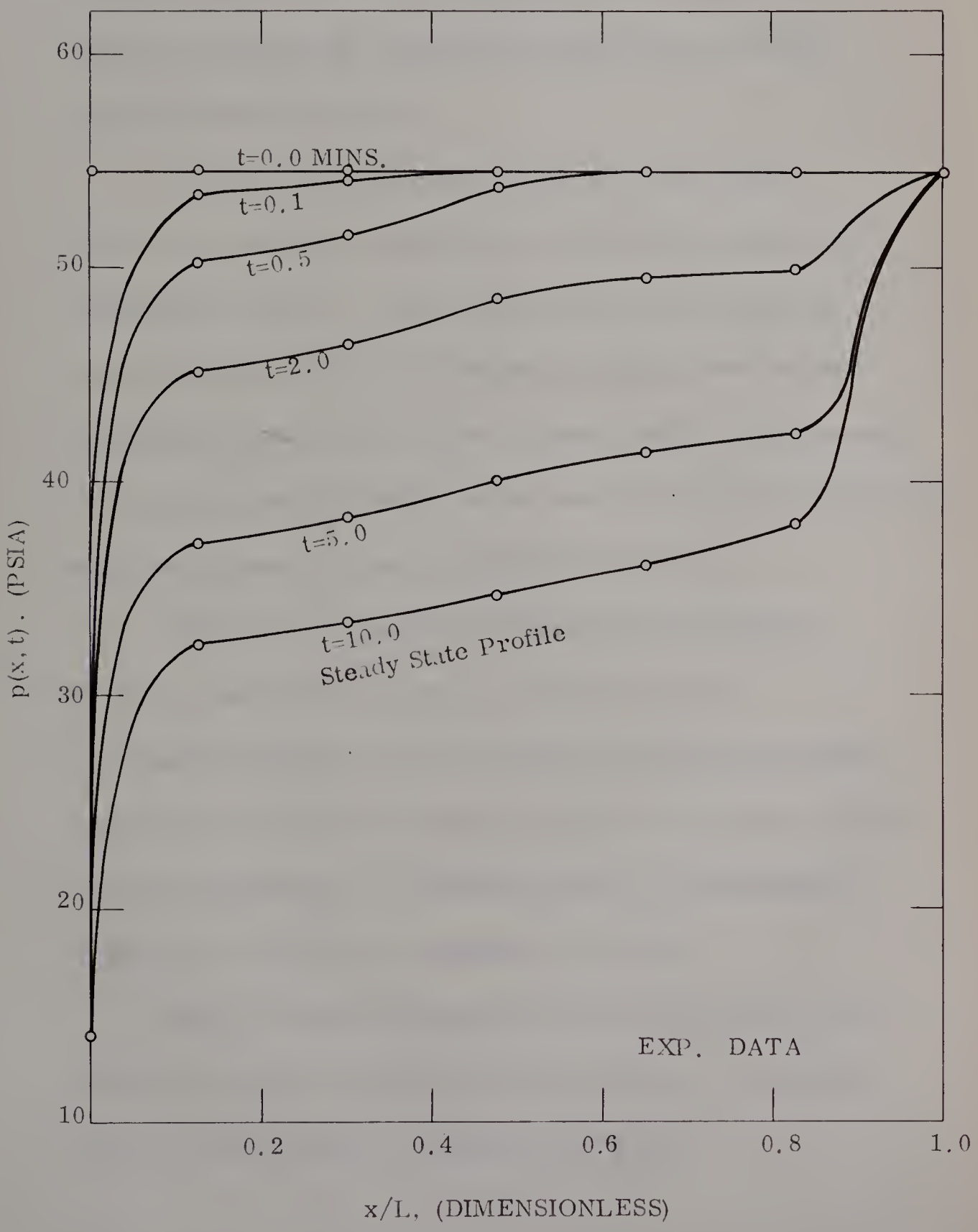

low permeability sections on each end of this core were due to machining of the end faces. In this study three-eights of one inch were fractured off each end before testing and obtaining results displayed in Figure 6.

A sample of further tests performed on the Berea 1 core but with additional rock volume removed from each end is illustrated in Figure 7. This modification more than doubled the permeability (see Table 2) but did not entirely remove the heterogeneous nature of the core. At steady state a large pressure drop associated with the tight section remained on the downstream end while the upstream end was considerably improved.

Figure 8 also depicts the heterogeneous behaviour of the Berea 1 and Berea 1A samples. Earlier assumptions that this behaviour was the result of damage incurred while machining the end face are disproved by this investigation. Either the sample was naturally very heterogeneous or it was damaged during earlier studies by a previous investigator.

One of the more homogeneous cores tested was the Berea 2 sample. A typical result is presented in Figure 9. Although this core was homogeneous it had such a high flow

FIGURE 7
PRESSURE DISTRIBUTION
BEREA 1A: CONSTANT TERMINAL PRESSURE WITH
CONSTANT PRESSURE AT EXTERNAL BOUNDARY

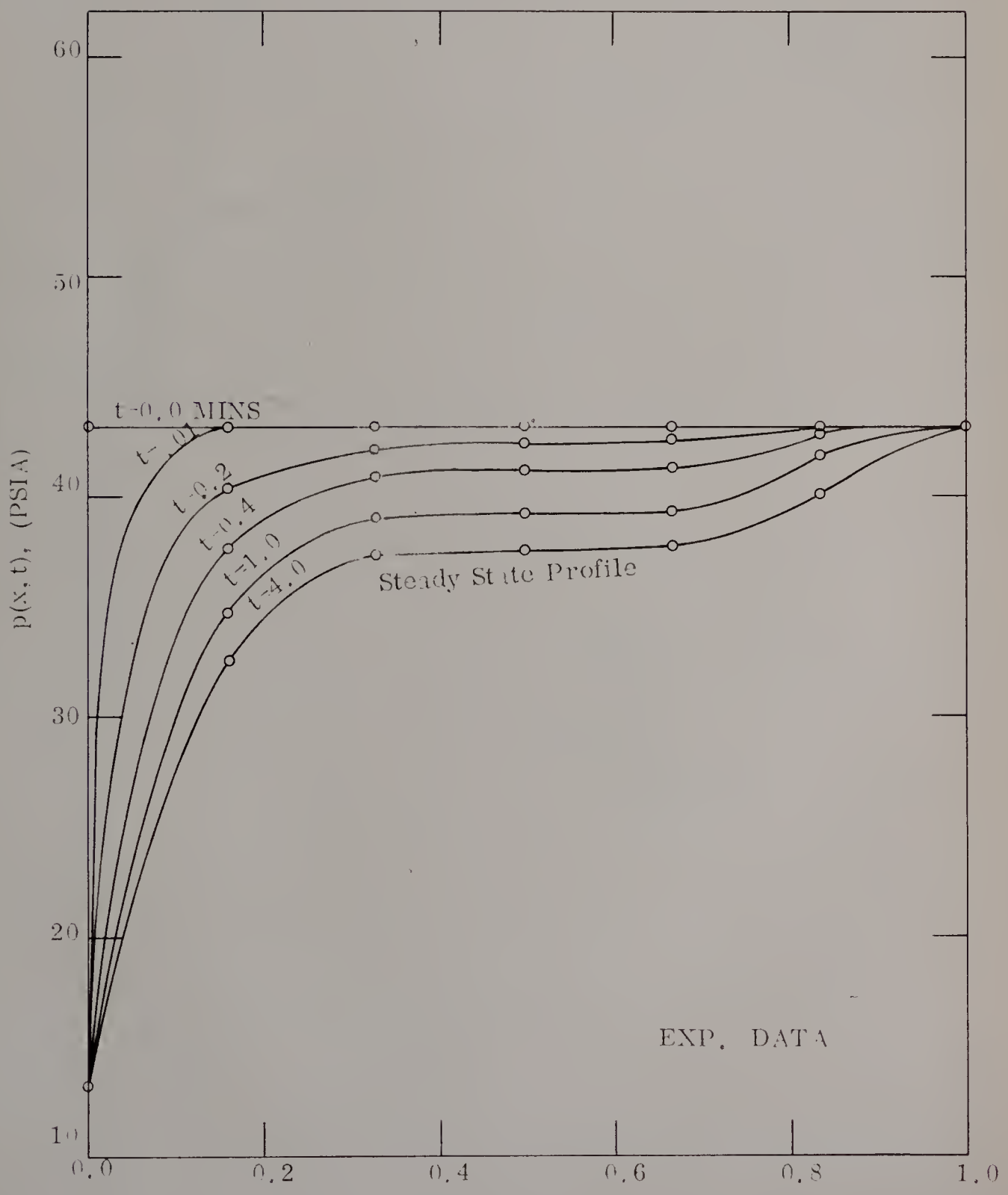

FIGURE 8
PRESSURE DISTRIBUTION

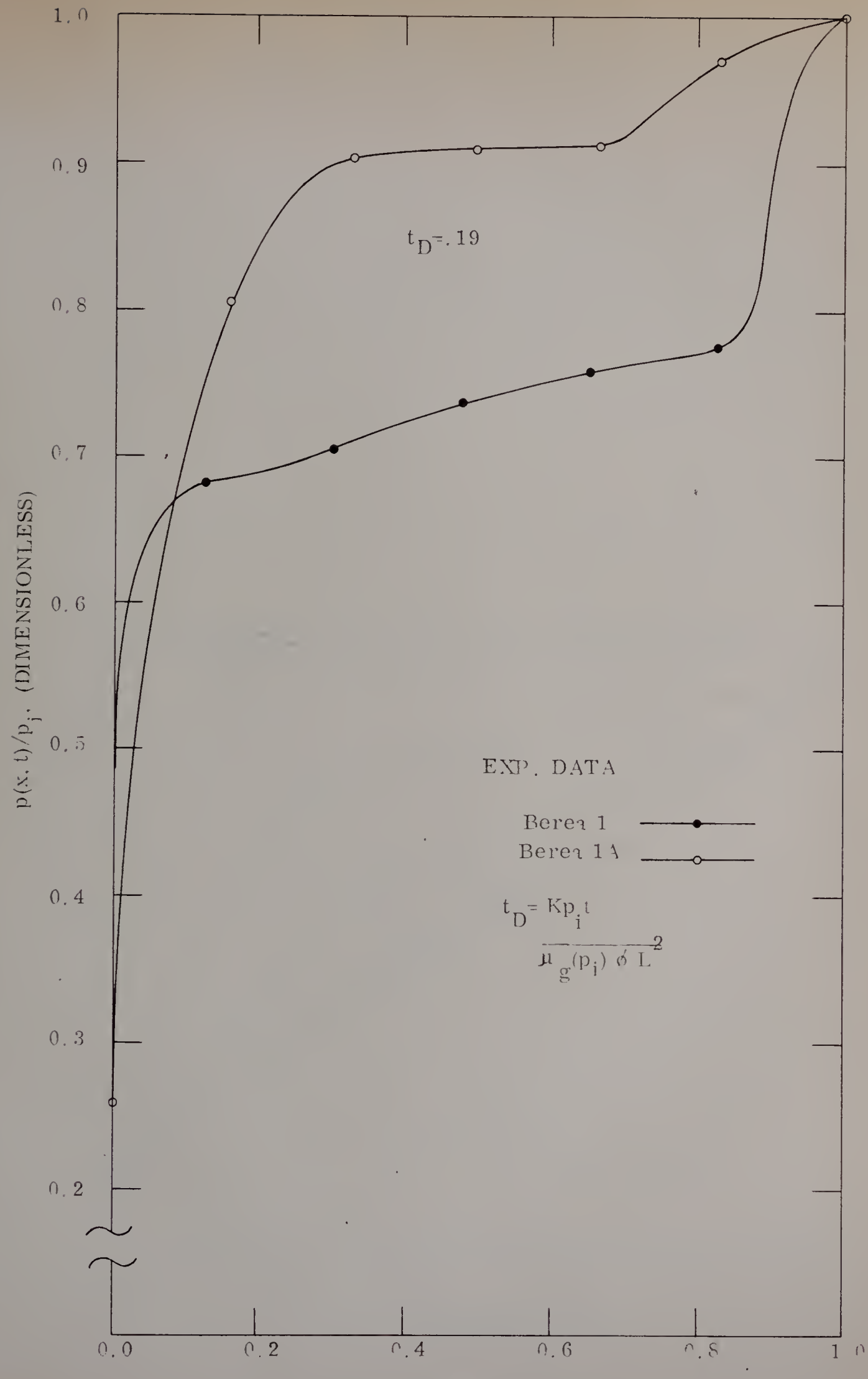

FIGURE 9
PRESSURE DISTRIBUTION
BEREA 2: CONSTANT TERMINAL PRESSURE WITH
CONSTANT PRESSURE AT EXTERNAL BOUNDARY

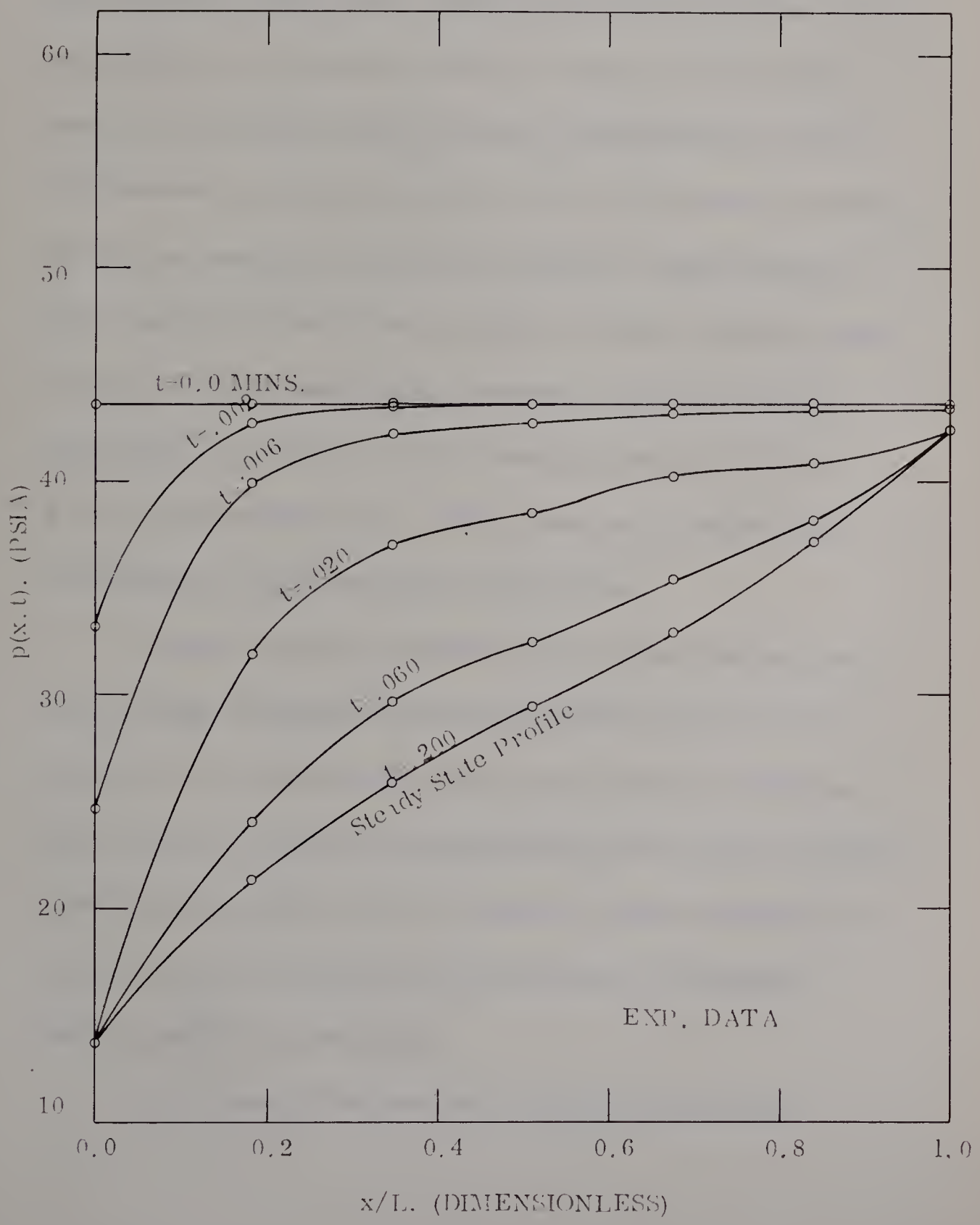

capacity, that constant terminal pressure could not be established prior to the transients reaching the upstream end of the core. Had this boundary condition been achieved instantaneously after opening the toggle valve, drawdown would have been more severe and a steady state condition would have been approached more rapidly. Furthermore, upon commencement of flow at the external boundary the high permeability contributed to high flow rates which could not be supplied by the pressure regulator without a slight pressure decline. From an experimental viewpoint, constant terminal rate would be a more appropriate boundary condition to study for this high capacity sample. Such a boundary condition might be achieved by a Moore constant rate regulator.

Another problem associated with the Berea 2 sample was the recording of negative pressure differentials by the upstream transducer while studying the second set of boundary conditions. This occurred at late time periods just prior to the system attaining a steady state condition. Such a behaviour might be attributed to a system leak at the upstream end of the core or transducer, however, neither was detected.

Typical results obtained while testing the Series core

which comprised of two different rock types, an Alundum section and a Berea sandstone section arranged in series, are presented in Figures 10 and 11. Figure 10 represents the unsteady state flow results when the Alundun Section was at the downstream end of the system while Figure 11 are results for the same sample but reversed, with the Berea section at the downstream end. These tests were intended to reveal the effect of a fracture in the Berea section and the discontinuity created by two different rock types. Unfortunately the taps were not spaced closely enough to detect the presence of the fracture nor were the permeabilities of the rock types sufficiently different to show the discontinuity. Furthermore, Figures 10 and 11 illustrate that the high capacity of the sample permitted the transients to reach the external boundary before constant terminal pressure could be achieved. However, the tests did illustrate that the core depleted initially much more rapidly when the tight section was at the downstream end as in Figure 10 than when reversed as in Figure 11. At t=0.5 minutes steady state conditions had not been attained in Figure 11 whereas they have in Figure 10.

As a check of the accuracy of the experimental results, a material balance based on the instantaneous pressure profiles observed was utilized to yield the dimensionless production function. The procedure involved numerical integration of the profiles to give average

FIGURE 10
PRESSURE DISTRIBUTION
SERIES CORE: ALUNDUM-BEREA
CONSTANT TERMINAL PRESSURE WITH CONSTANT PRESSURE
AT THE EXTERNAL BOUNDARY

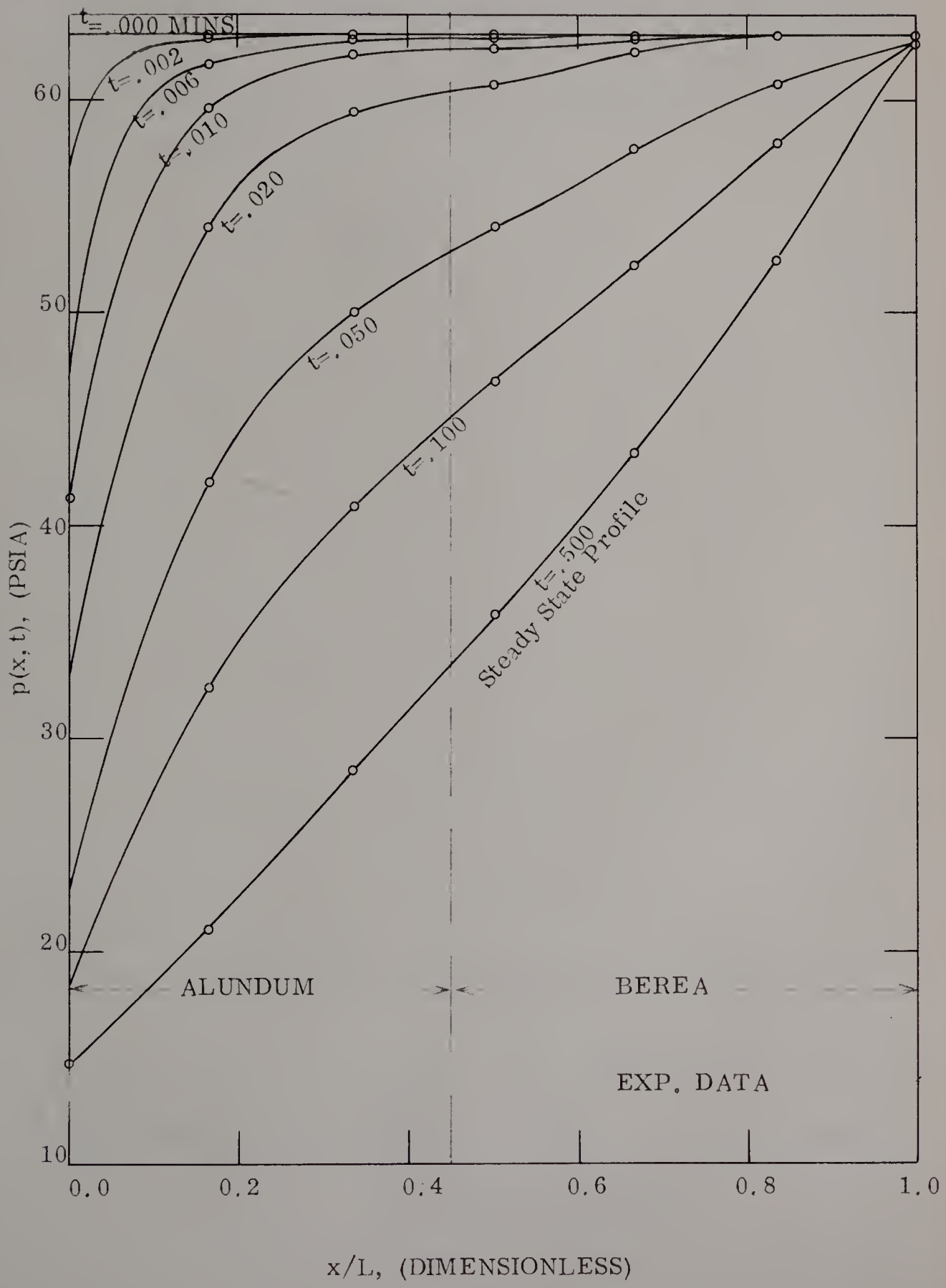

FIGURE II
PRESSURE DISTRIBUTION
SERIES CORE: BEREA-ALUNDUM
CONSTANT TERMINAL PRESSURE WITH CONSTANT
PRESSURE AT EXTERNAL BOUNDARY

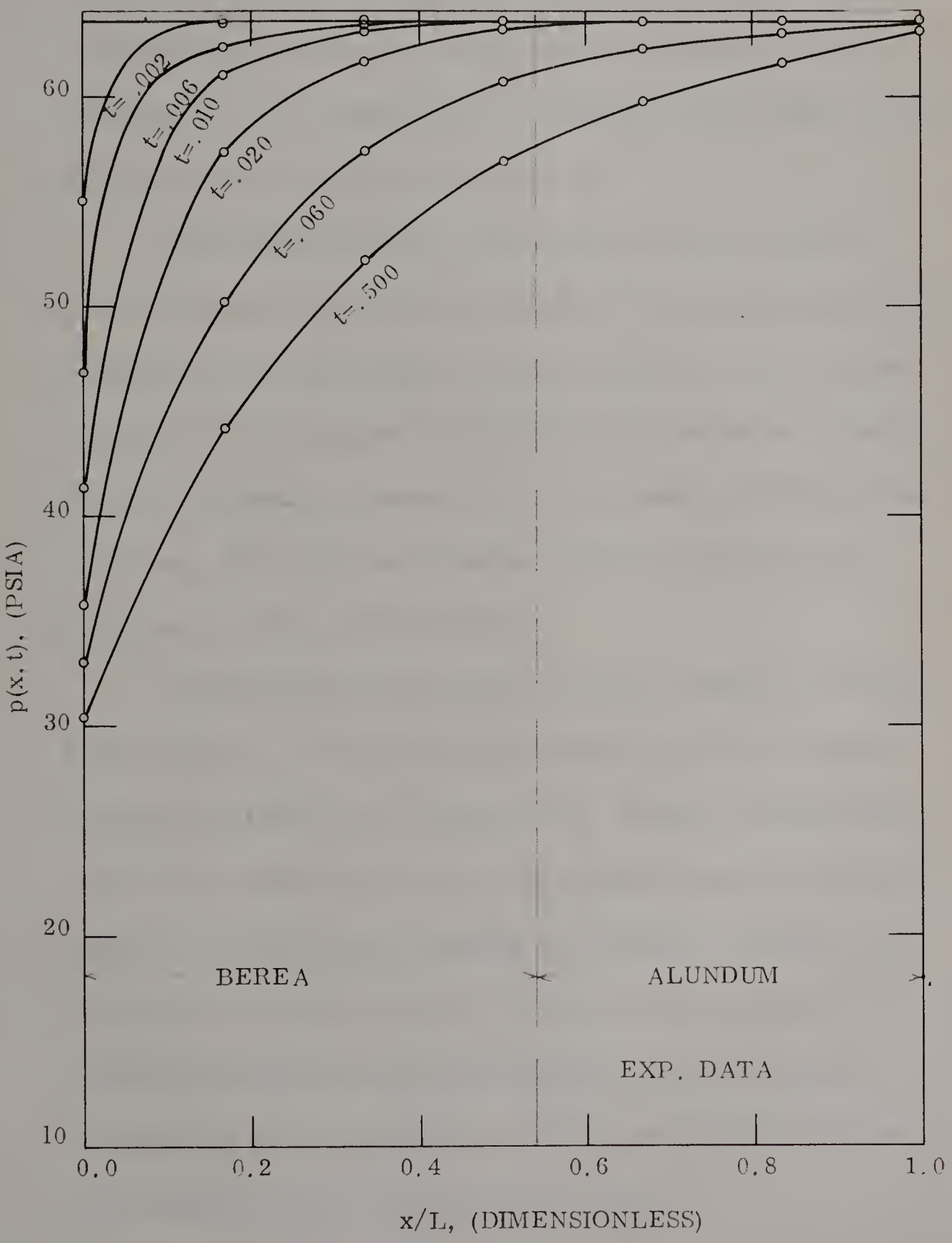

pressures which when utilized in a material balance yielded cumulative production for times corresponding to the profiles. Once obtained these were converted to dimensionless production as defined by Van Everdingen and Hurst [31]. All calculations were performed on the digital computer and the results are presented in Figure 12.

As the theory predicts, dimensionless production from all cores regardless of its physical properties are coincidential at dimensionless times corresponding to an infinite behaviour of the system. Subsequent to the transients reaching the finite boundaries, departure from the infinite curve seemed to occur commencing with the shorter specimens. The minor discrepancies noted are attributed to non-homogeneities of the systems studied.

The heterogeneous behaviour of the core samples is exemplified in Figure 13. This type of dimensionless plot should bring all the pressure profiles on to a single curve. However, because there was no theoretically valid means of expressing dimensionless time to account for variation of permeability with position, deviations from the common curve were observed. The permeability used in evaluating dimensionless time as plotted along the abscissa in Figure 12 and Figure 13 was the average liquid or absolute permeability of the entire core as determined from steady state flow data.

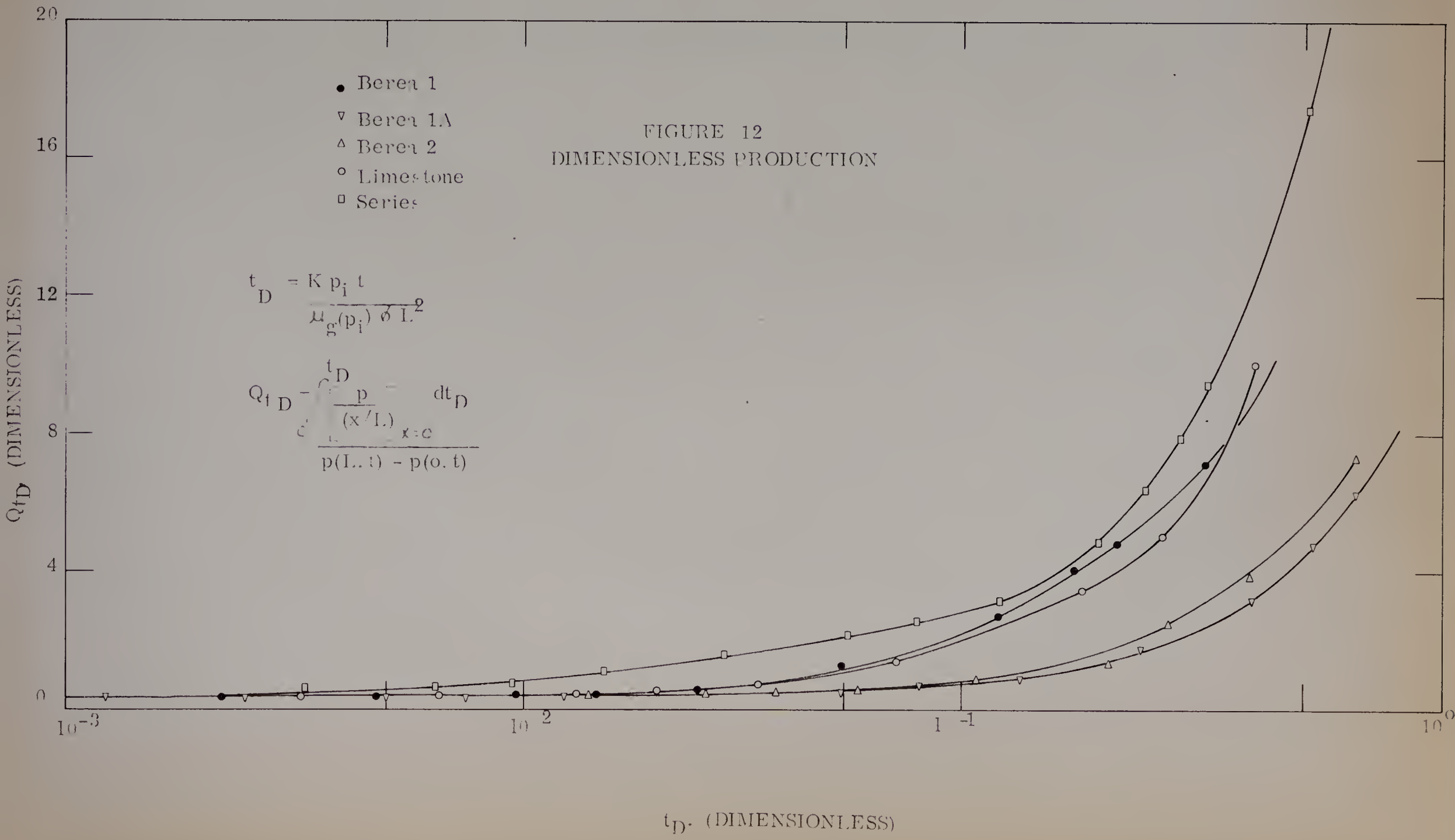

FIGURE 12
DIMENSIONLESS PRODUCTION

FIGURE 13

DIMENSIONLESS PRESSURE DISTRIBUTION

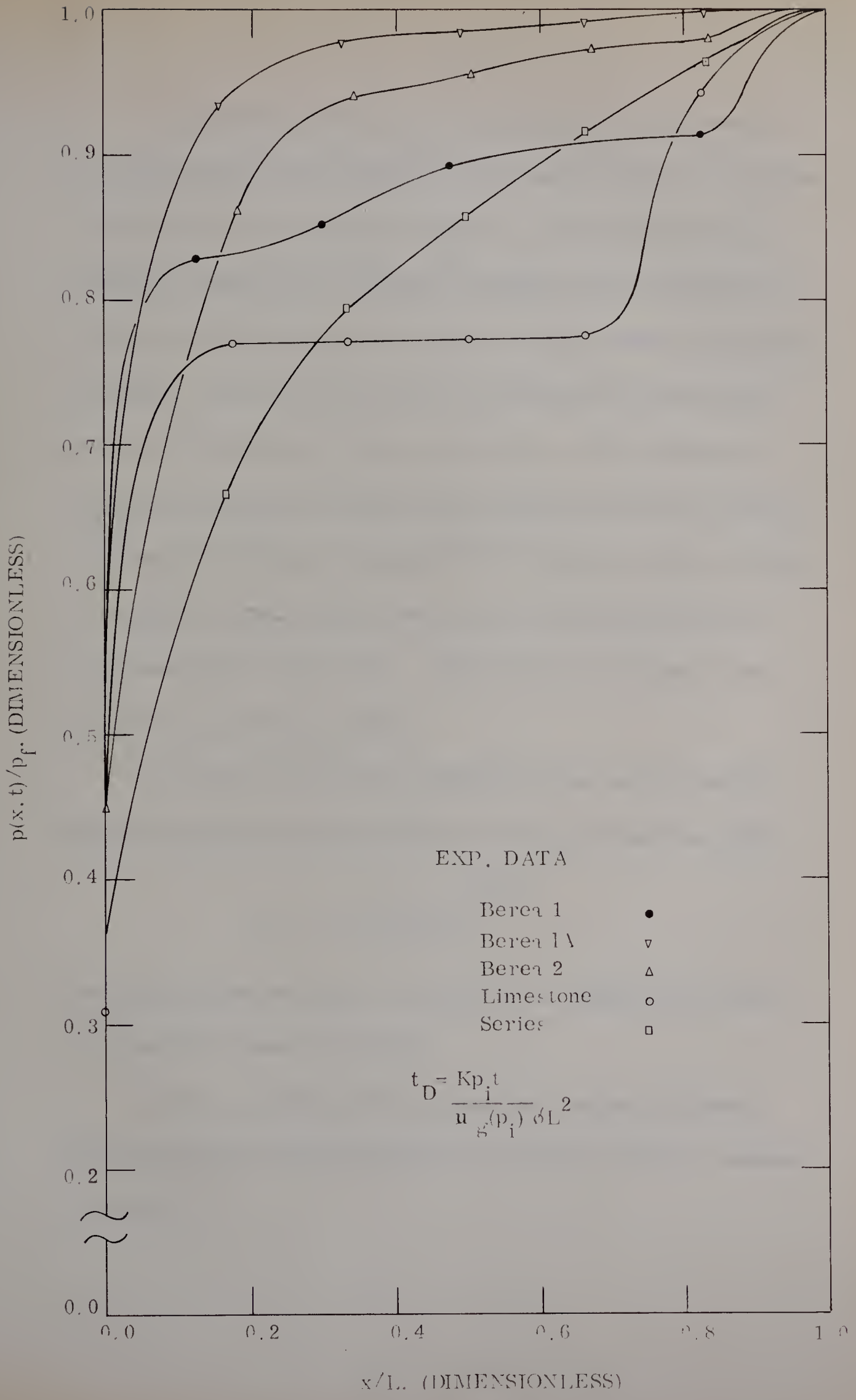

An additional check of the experimental data was provided by a comparison of the stabilization time and the physical properties of each system as presented in Figure 14. The stabilization time which was obtained from visicorder readings represented the time that each and every point in the system had approached a steady state condition. That is, the time when the pressure drop across each section had stabilized to some constant value. The grouping of physical properties as plotted on the ordinate was based on correlations summarized by Van Poolen [32]. These correlations implied a straight line relationship which seems to be confirmed by the experimental data of this study. Each data point pertains to one of the five flow systems studied.

For linear systems the stabilization time can be predicted by the following correlation which was developed from this study:

$$ts = 1.31\left[\frac{\phi L^2}{K}\right]^{.344}$$

Permeability has the units of millidarcies and length has the units of inches while time is in minutes.

Such a correlation will facilitate the planning of unsteady state flow tests provided the physical properties of the flow systems are known.

FIGURE 14
STABILIZATION TIME

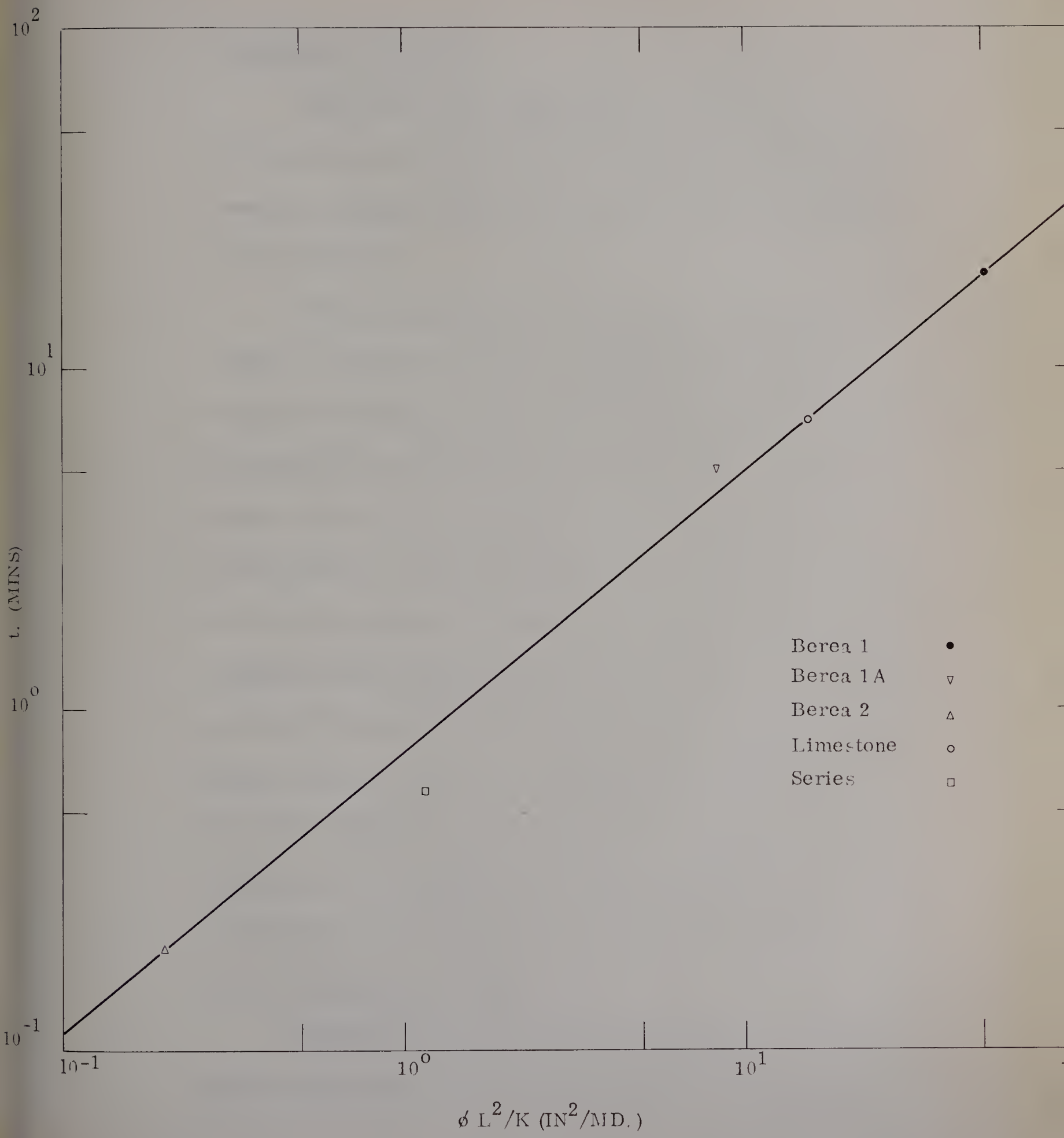

NUMERICAL SOLUTIONS

A duplication of the experimental results was achieved by solving the partial differential equation describing gas flow by the numerical technique presented in an earlier section and developed in the Appendices.

Accuracy of the numerical solution for a homogeneous system is illustrated in Figure 15 through a comparison with an analytical solution presented in Katz[18]. Discrepancies between the numerical and analytical solutions show a trend of going from positive deviations to increasingly more negative deviations as time increases. A further comparison could not be made because the pressure profiles have reached the external boundary and the analytical solution applies only to an infinite system. A comparison performed on data for the other samples revealed similar discrepancies; however, there was no consistency as to whether the numerical solutions were greater than or less than the analytical solution for a corresponding time. If the discrepancies were consistently in one direction they might suggest some inherent error in the mathematical model.

Utilizing the average Klinkenberg permeability of each core and the mathematical model, pressure profiles for homogeneous

FIGURE 15
BEREA 1
PRESSURE DISTRIBUTION

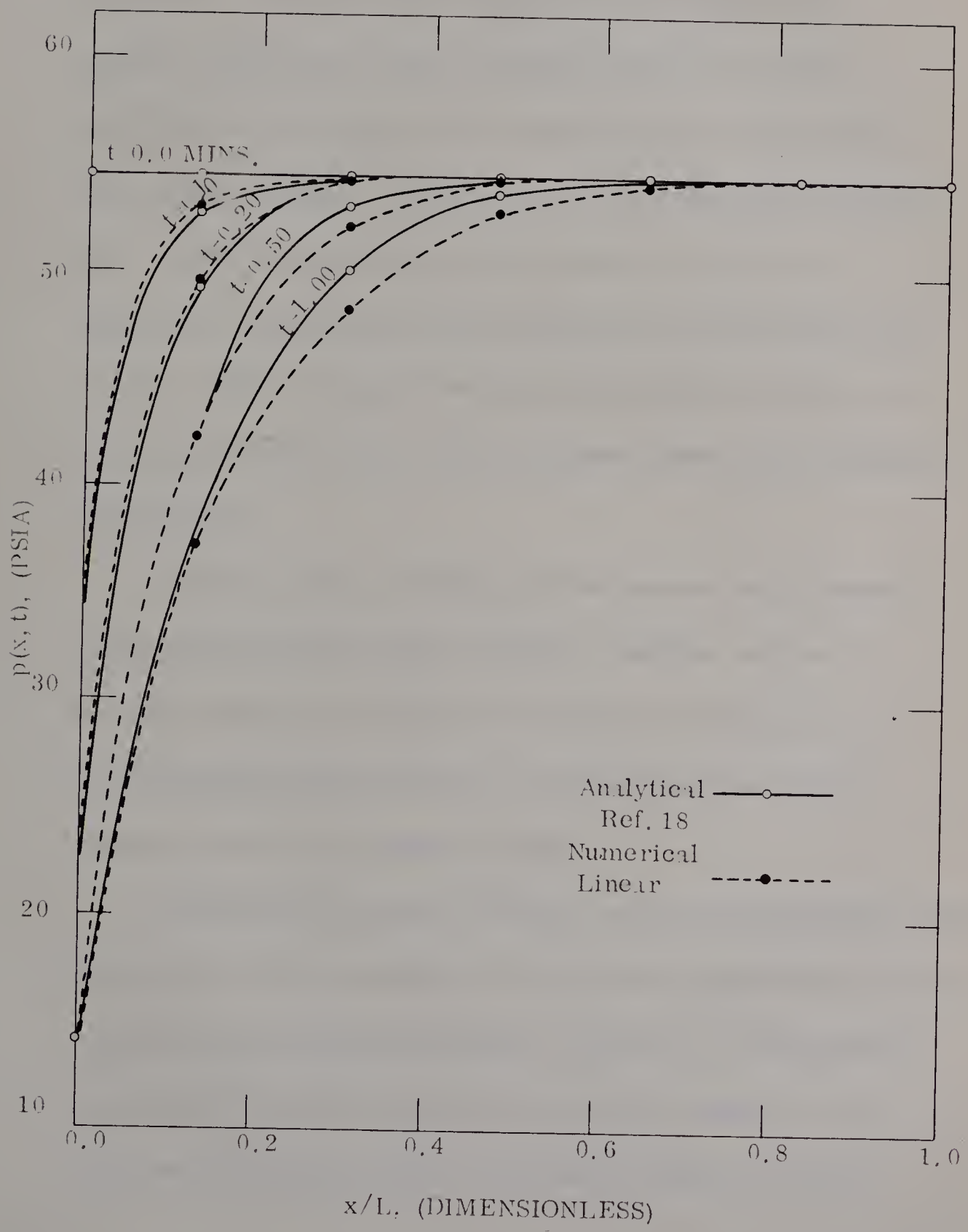

systems were calculated. One such profile is illustrated in Figure 16. The ordinate is a dimensionless pressure term $p(x,t)/p_i$, which is the ratio of pressure change at any point within the porous medium to the constant pressure maintained at the external boundary. The abscissa is the dimensionless distance, x/L. Unlike the experimental data presented in Figure 13, a single curve was obtained with the exception of that for the Berea 2 core. Figure 16 supports the theoretical aspects of such a plot and illustrates the effects of heterogeneous systems when compared with Figure 13.

The Berea 2 data deviates from the common curve because the constant terminal pressure boundary condition, common to the other tests, was not attained immediately, consequently at a corresponding dimensionless time, depletion was less and the pressure profile was resultantly higher.

Extending the numerical technique to the non-homogeneous systems by using the actual permeability of each section studied experimentally, results in the comparison presented in Figure 17. The numerical approximation coincided with the experimental results for early times but deviates positively in the interior sections as steady

FIGURE 16
DIMENSIONLESS PRESSURE DISTRIBUTION

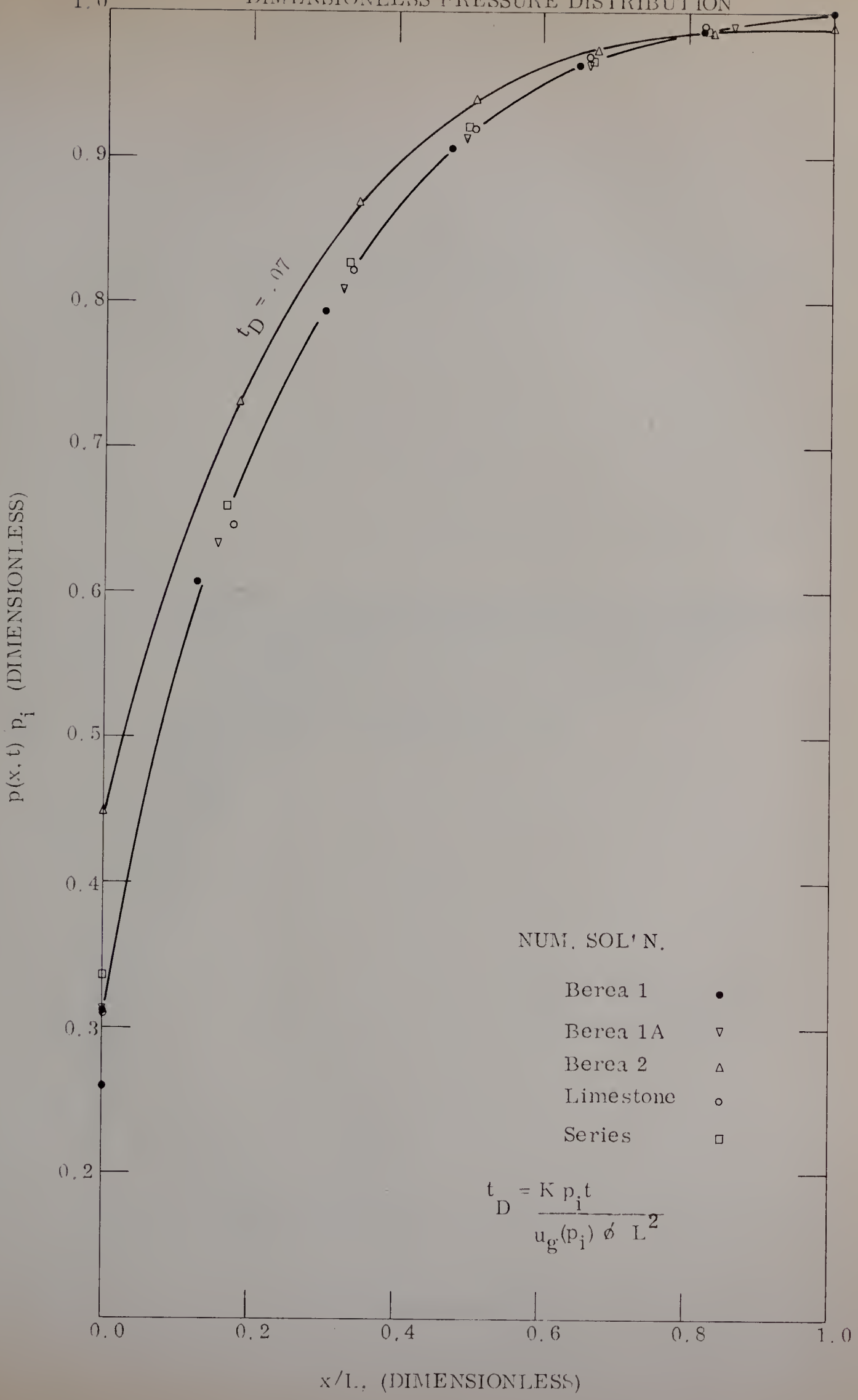

FIGURE 17
PRESSURE DISTRIBUTION
BEREA 1A: CONSTANT TERMINAL PRESSURE WITH
CONSTANT PRESSURE AT EXTERNAL BOUNDARY

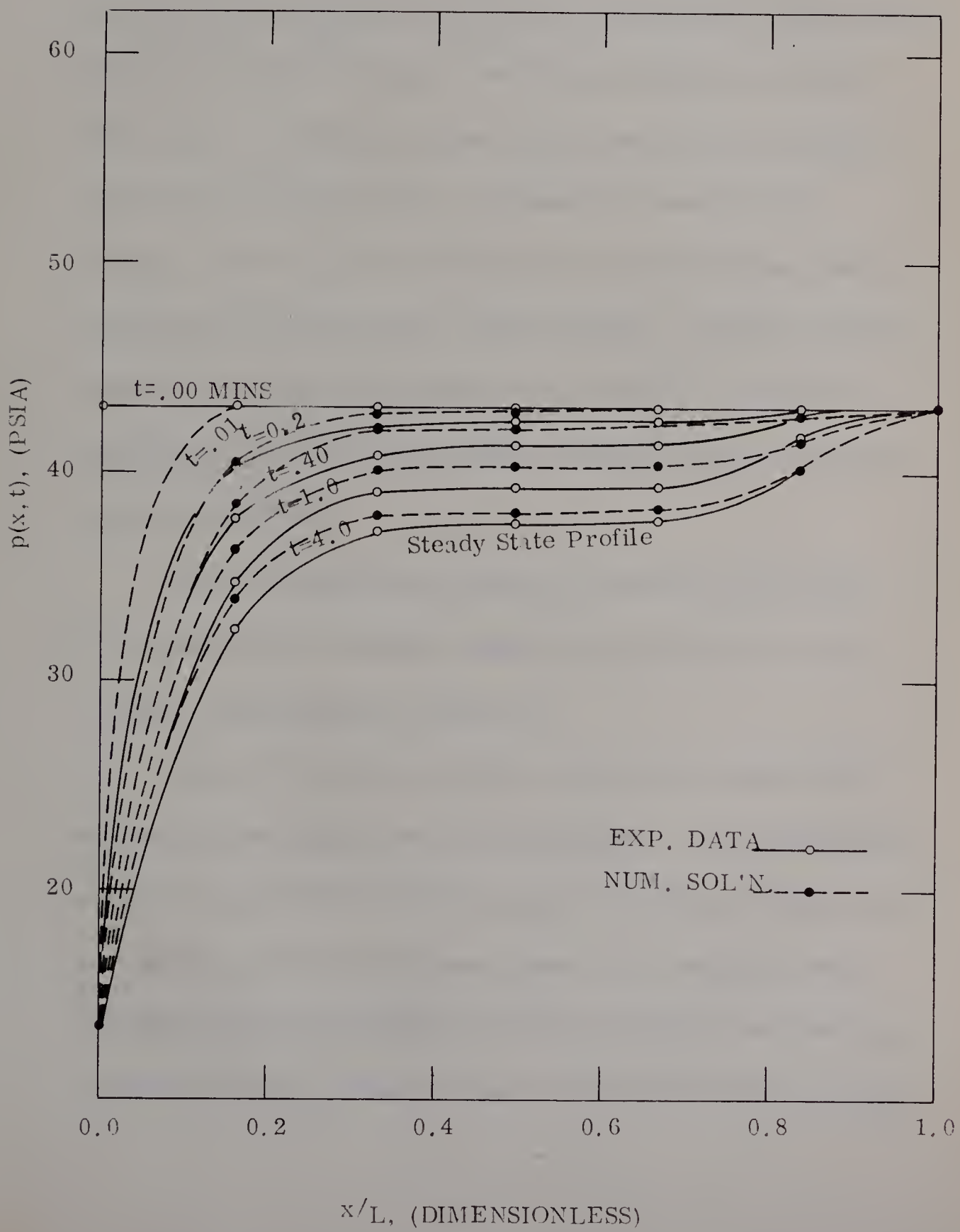

state conditions were approached. At flow periods as short as t=0.2 minutes, it was apparent that the depletion of the system as predicted by the numerical solution was less than that experimentally observed. Chwyl [10] who by a numerical technique was able to examine the contributions of gas slippage and inertia individually also observed this phenomena. Molecular streaming or gas slippage, which was not accounted for in the mathematical model, was the most apparent cause of such behaviour. However utilizing Chwyl's data, slippage accounted for only about 0.1 psi of the discrepancy. Using the same source, inertial effects were calculated to be negligible.

Similar deviations are observed when comparing results for the second set of boundary conditions as applied to the Berea 1A sample and presented in Figure 18.

Figure 19 compares results for the Berea 2 sample which experienced the highest flow rates encountered. For corresponding time, the experimental data were greater than the numerical solution, just opposite to the previous comparison. This behaviour can be explained by the fact that higher internal pressures were necessary to provide sufficient pressure drop to overcome the inertial effects.

FIGURE 18
PRESSURE DISTRIBUTION
BEREA 1A: CONSTANT TERMINAL PRESSURE WITH
SEALED EXTERNAL BOUNDARY

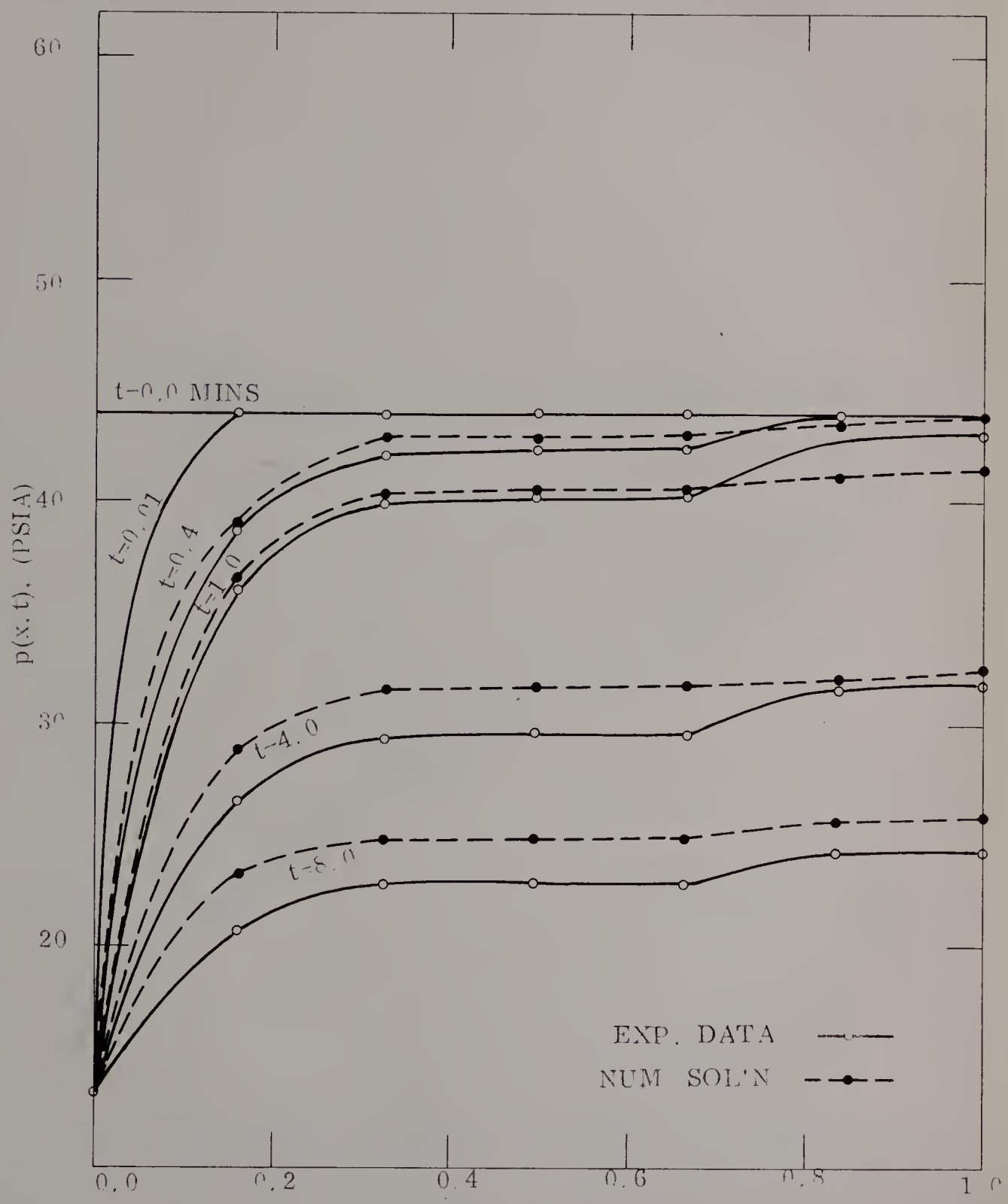

FIGURE 19
PRESSURE DISTRIBUTION
BEREA 2: CONSTANT TERMINAL PRESSURE WITH
CONSTANT PRESSURE AT EXTERNAL BOUNDARY

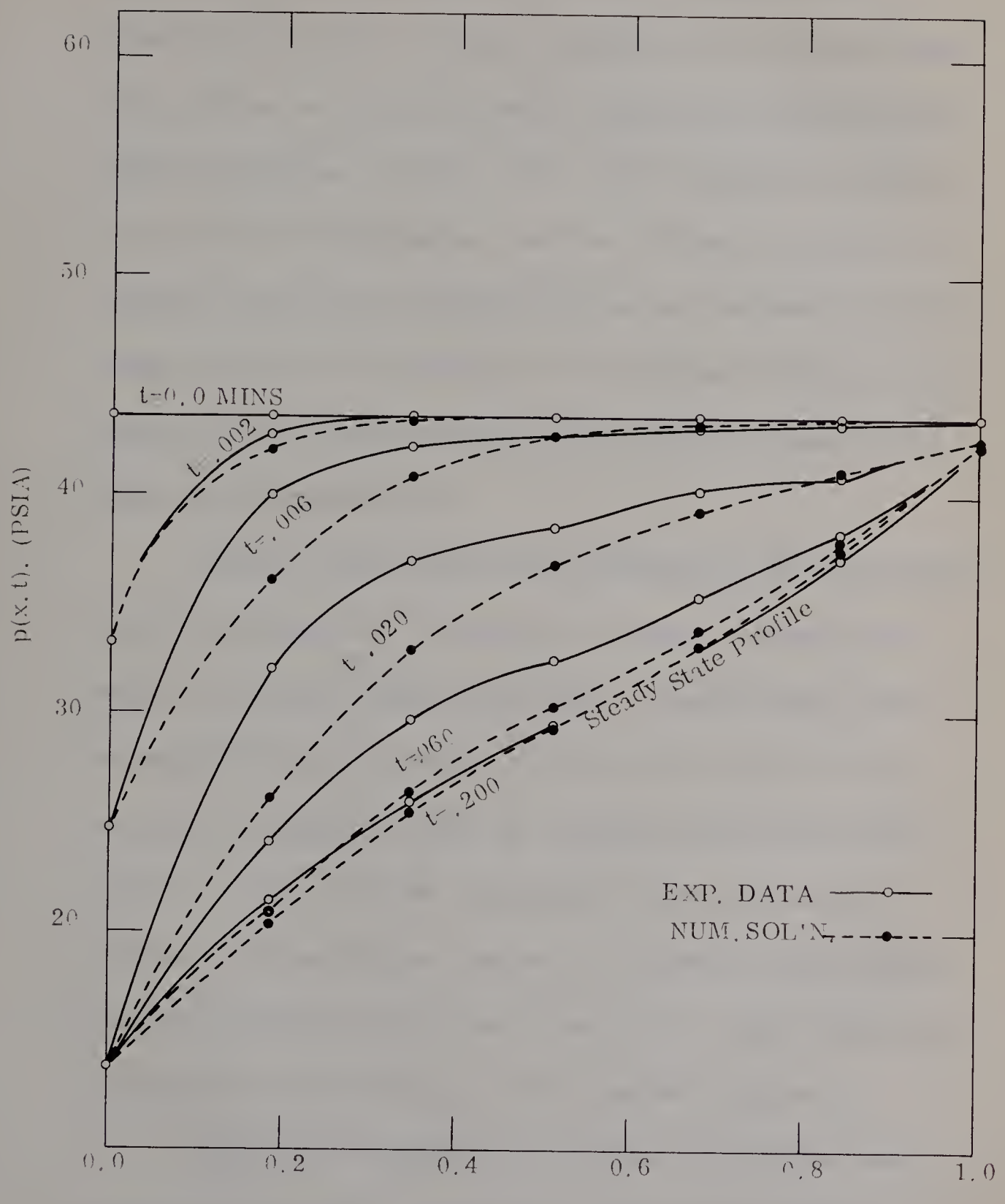

not considered in the mathematical model. Evaluation of the dimensionless inertial resistance coefficient and the dimensionless slip coefficient as defined by Chwyl, revealed these inertial effects might be significant. However, their actual quantitative contribution towards the discrepancies observed in Figure 19 could not be evaluated because of the exponential behaviour displayed by Chwyl's results and the need to interpolate. Nevertheless, from qualitative aspects it appeared that Chwyl's results would not account for the entire disrepancy observed.

Additional factors which would contribute to the discrepancies observed in Figures 17, 18 and 19 are erroneous permeabilities and/or an incorrect mathematical model. Possible errors in the permeability data arise because of the limited amount of steady state data available to evaluate the variation of permeability with position. In the case of the mathematical model, the method of discretizing the derivatives resulted in an equation which produced a non-symmetrical matrix of non-linear terms. Such a matrix could yield cyclic results which may be the situation in Figure 18.

Experimental and numerical solutions for the other core samples are presented in Appendix D, Figures D-8 through to Figure D-10.

CONCLUSIONS

From observations made and results obtained in the course of this investigation, the following conclusions were formulated.

1. The mathematical model developed for linear systems can be solved numerically to give results approximating those experimentally observed. Deviations between results can be attributed to molecular streaming, inertial effects, erroneous permeabilities and/or inherent errors in the model.

2. No valid means of expressing dimensionless time to account for variation of permeability with position in a linear system exists.

3. Pressure distributions obtained experimentally for the two sets of boundary conditions are identical for each system until the pressure disturbance created at the down-stream end reaches the upstream end.

4. The Series sample, designed to simulate non-homogeneous behaviour, is not heterogeneous enough and possesses too high a flow capacity for optimum transient study.

5. The excessive pressure differentials observed across each end of the Berea 1 sample are not attributable to mechanical end effects but arise as a result of damage incurred in a previous investigation.

6. Long core samples are desirable. Lengths in excess of five feet facilitate the measurement of transients.

7. Core samples with an absolute permeability in excess of 100 millidarcies are undesirable for transient flow tests. This type of sample makes it difficult to simulate the boundary conditions examined in this study.

RECOMMENDATIONS

1. More representative transient pressure measurement might be obtainable by drilling more than one pressure tap at each location along the length of the flow system.
2. Numerous steady state flow tests should be performed on each core sample to facilitate the evaluation of the permeability of each section of the sample.
3. When estimating time required to conduct transient flow tests, the correlation developed in this study relating stabilization time to physical properties should be employed.
4. The boundary condition of constant terminal rate should be investigated because it has more practical applications and it might facilitate the transient study of higher capacity samples.
5. The mathematical model should be modified to incorporate molecular streaming and inertial effects, and perhaps obtain a better approximation to the experimental results.

NOMENCLATURE

$[A]$	matrix of non-linear terms
$\vec{b}$	vector of known terms
K	absolute (liquid) permeability (L^2)
k	permeability (L^2)
k_g	gas permeability (L^2)
L	overall length of linear system (L)
M	molecular weight (m)
p	pressure (m/Lt^2)
$\vec{p}$	vector of unknown pressures (m/lt^2)
p_i	initial pressure (m/Lt^2)
p_w	pressure at the producing end (m/Lt^2)
R	universal gas constant (mL^2/t^2T)
t	time (t)
ts	stabilization time (t)
T	temperature (T)
$\vec{v}$	volumetric flow rate per unit cross-sectional area (L/T)
W	inverse of product of viscosity and compressibility $(\frac{Lt}{m})$
x	distance along linear axis (L)
z	gas compressibility factor
μ	viscosity (m/Lt)
μ_g	gas viscosity (m/Lt)

ρ density (m/L^3)

ρ_g gas density (m/L^3)

ϕ porosity

SUBSCRIPTS

g gas

i initial value or conditions

j grid point index along length

k grid point index along time

s stabilization

w producing end of the system

SUPERSCRIPTS

$\rightarrow$ denotes vector quantity

r index of iteration number

$-$ denotes a mean value

MATHEMATICAL NOTATION

∇ del operator (gradient)

Δ delta difference

$\nabla\cdot$ divergence

$\partial/\partial y$ partial derivative with respect to y

BIBLIOGRAPHY

1. Al-Hussainy, R., Ramey, H. J. Junior, and Crawford, P.B.: "The Flow of Real Gases Through Porous Media", J. Petrol. Tech., May 1966, p. 624.

2. Aronofsky, J. S. and Jenkins, R.: "Unsteady Flow of Gas through Porous Media: One Dimensional Case", Proc. 1st, U.S. Nat'l. Congr. Appl. Mech., 1952, p. 763.

3. Aronofsky, J. S. and Jenkins R.: "Unsteady Radial Flow of Gases Through Porous Media", J. Appl. Mech., Vol. 20, 1953, p. 210.

4. Aronofsky, J. S. and Ferris, O. D.: "Transient Flow of Non-ideal Gases in Porous Solids: One-dimensional Case", J. Appl. Physics, Vol. 25, 1954, p. 289.

5. Aronofsky, J. S. and Porter, J. D.: "Unsteady Radial Flow of Gas Through Porous Media: Variable Viscosity and Compressibility", J. Appl. Mech., Vol. 23, 1956, p. 128.

6. Bruce, G.H., Peaceman, D.W., Rachford, H.H. and Rice, J.D.: "Calculation of Unsteady-State Gas Flow Through Porous Media", Trans. AIME, Vol. 198, 1953, p. 79.

7. Cachero, A.: M. Sc. Thesis in process of completion, University of Alberta, Edmonton, 1968.

8. Carter, R. D.: Performance Prediction for Gas Reserves Considering Two-dimensional Unsteady-State Flow, Trans. AIME, Vol. 237, 1966, p. 35.

9. Churchill P.V.: "Modern Operational Mathematics in Engineering", McGraw-Hill Book Co., Inc., New York, 1944.

10. Chwyl, E.: "An Analysis of Transient Gas Flow Through Porous Media", M.Sc. Thesis, University of Alberta Edmonton, February, 1968.

11. Dranchuk, P.M. and Sadiq, S.: "The Interpretation of Permeability Measurements", J. Can. Petrol. Tech., Vol. 4, No. 3, 1965, p. 130.

12. Dranchuk, P.M., and Kolada, L.J.: "Interpretation of Steady Linear Visco-Inertial Gas Flow Data", paper presented at the 18th Annual Technical Meeting of the Petroleum Society of CIM, May, 1967.

13. Eilerts, K.C.: "Integration of Partial Differential Equation for Transient Linear Flow of Gas Condensate Fluids in Porous Structures", Soc. Pet. Engrs. J., Vol. 4, No. 4, December 1964, p. 291.

14. Hamilton, R.J.: "A Study of Linear, Steady State, Gas Flow Through Consolidated Porous Media", M.Sc. Thesis, University of Alberta, Edmonton, February, 1965.

15. Hetherington, C.R., MacRoberts, D.T., and Huntington, R.L.: "Unsteady Flow of Gas Through Porous Media", Trans AIME, Vol. 146, 1942, 1. 166.

16. Hilsenrath, J., Becket, C.W., Benedict, W.S., Fano, L., Hoge, H.J., Masi, J.F., Toylavkian, Y.S., and Wooley, H.W.: "Tables of Thermal Properties of Gases", National Bureau of Standards, Washington, D.C., Circular 554, 1955, Table 7-1, p. 317.

17. Hubbert, M.K.: "Darcy's Law and the Field Equations of the Flow of Underground Fluids", Trans AIME, Vol. 37, 1956, p. 222.

18. Katz, D.L., Cornell, D., Kobayashi, R., Poettmann, F.H., Vary, J.A., Elenbaas, J.R., and Weinaug, C.F.: "Handbook of Natural Gas Engineering", McGraw-Hill Book Co., Inc., New York 1959, Chapter 10.

19. Kestin, J. and Wong, H.E.: "The Viscosity of Five Gases: A Re-Evaluation", Trans A.S.M.E., Vol. 80, 1958, Table 1, p. 13.

20. Kidder, R.E.: "Unsteady Flow of Gas Through Semi Infinite Porous Medium", ASME, J. of Appl. Mech. Vol. 24, March 1957, p. 392.

21. Klinkenberg, L.J.: "The Permeability of Porous Media to Liquids and Gases", Drill. and Prod. Proc., API, 1941, p. 200.

23. Lapidus, L.: "Digital Computation for Chemical Engineers", McGraw-Hill Book Co., Inc., 1962, Chapter 4.

23. Mackett, R.A.: "Viscous and Viscous Interial Gas Flow In Limestone Cores", M.Sc. Thesis, University of Alberta, Edmonton, November, 1966.

24. Muskat, M.: "Flow of Homogeneous Fluids", McGraw-Hill Book Co., Inc., New York, 1937, Chapter 7.

25. Quon, D.,Dranchuk, P.M., Allada, S.K. and Leung, P.K.: "A Stable, Explicit, Computationally Efficient Method for Solving Two-Dimensional Mathematical Models of Petroleum Reservoirs", J. Can. Pet. Tech., Vol. 4, No. 2, 1965, p. 330.

26. Quon, D., Dranchuk, P.M., Allada, S.R. and Leung, P.K.: "Application of the Alternating Direction Explicit Procedure to Two-Dimensional Natural Gas Reservoirs", Soc. Pet. Eng. J., June, 1966, p. 137.

27. Ralston, A.: "A First Course in Numerical Analysis", McGraw-Hill Book Co., Inc., New York, 1965, Chapter 8.

28. Roberts, R.C.: "Unsteady Flow of Gas Through a Porous Medium", Proc. 1st U.S. Nat'l. Congr. Appl. Mech., 1952, p. 773.

29. Scheidegger, A.E.; "The Physics of Flow Through Porous Media", University of Toronto Press, Toronto, 1957.

30. Steel, D.I., and Orbach, L.B.: "Theory and Use of the Vol-O-Flow Meter", National Instrumental Laboratories Publication, January, 1963.

31. Van Everdingen, A.F. and Hurst, W.: "The Application of the Laplace Transformation to Flow Problems in Reservoirs", Trans. AIME, Vol. 186, 1949, p. 305.

32. Van Poolen, H.K.: "Radius of drainage and stabilization time equations", Oil Gas J., September, 1964, p. 138.

APPENDIX A

DERIVATION OF THE GAS FLOW MATHEMATICAL MODEL

DERIVATION OF GAS FLOW MATHEMATICAL MODEL

The continuity equation for a compressible fluid may be written as:

$$\left[\begin{array}{l}\text{Amount of}\\ \text{Mass Input}\end{array}\right] - \left[\begin{array}{l}\text{Amount of}\\ \text{Mass Output}\end{array}\right] = \left[\begin{array}{l}\text{Increase of Mass}\\ \text{Within the Region}\end{array}\right]$$

or in mathematical terms, this material balance based on conservation of mass for isothermal fluid flow through a porous medium is:

$$\nabla \cdot \left[\rho \vec{v}\right] = - \phi \frac{\partial \rho}{\partial t} \qquad \text{(A-1)}$$

Assuming flow to be laminar and horizontal, the velocity vector in Equation (A-1) may be expressed by Darcy's law:

$$\vec{v} = \frac{-k(p)}{\mu(p)} \nabla p$$

Substituting this into Equation (A-1) for the velocity vector yields:

$$\nabla \cdot \left[-\rho \frac{k(p)}{\mu(p)} \nabla p\right] = - \phi \frac{\partial \rho}{\partial t} \qquad \text{(A-2)}$$

Since the fluid being considered is a real gas, the density terms in Equation (A-2) may be represented respectively by the following forms of the equation of state:

$$\rho_g = \frac{M}{RT} \left[\frac{p}{z(p)}\right]$$

and

$$\frac{\partial \rho_g}{\partial t} = \frac{M}{RT} \frac{\partial}{\partial t}\left[\frac{p}{z(p)}\right]$$

which when substituted into Equation (A-2) gives:

$$\nabla\cdot\left[\frac{-M}{RT}\left\{\frac{k_g(p)\,p}{\mu_g(p)\,z(p)}\right\}\nabla p\right] = \frac{-M}{RT}\,\phi\,\frac{\partial}{\partial t}\left[\frac{p}{z(p)}\right] \qquad \text{(A-3)}$$

Since M/RT is constant for isothermal variation of pressure it cancels as do the negative signs yielding:

$$\nabla\cdot\left[\frac{k_g(p)}{\mu_g(p)\,z(p)}\,p\nabla p\right] = \phi\,\frac{\partial}{\partial t}\left[\frac{p}{z(p)}\right] \qquad \text{(A-4)}$$

In this study involving very heterogeneous cores, the permeability was considered a function of position only, independent of any pressure variation. Furthermore, the systems were linear therefore the resulting equation is:

$$\frac{\partial}{\partial x}\left[\frac{K(x)\,p}{\mu_g(p)\,z(p)}\,\frac{\partial p}{\partial x}\right] = \phi\,\frac{\partial}{\partial t}\left[\frac{p}{z(p)}\right] \qquad \text{(A-5)}$$

If a pressure function is introduced such that:

$$W(p) = \frac{1}{\mu_g(p)\,z(p)}$$

Equation (A-5) reduces to a non-linear partial differential equation of the form:

$$\frac{\partial}{\partial x}\left[W(p)\ K(x)\ p\ \frac{\partial p}{\partial x}\right] = \phi\ \frac{\partial}{\partial t}\left[\frac{p}{\mathcal{Z}(p)}\right] \qquad \text{(A-6)}$$

Further modifications involve the introduction of a mean pressure term on the right-hand side of Equation (A-6) and utilizing the equivalents

$$2p\ \frac{\partial p}{\partial x} = \frac{\partial p^2}{\partial x} \quad \text{and} \quad 2p\ \frac{\partial p}{\partial t} = \frac{\partial p^2}{\partial t}$$

to yield:

$$\frac{\partial}{\partial x}\left[W(p)\ K(x)\frac{\partial p^2}{\partial x}\right] = \frac{\phi}{p}\ \frac{\partial}{\partial t}\left[\frac{p^2}{\mathcal{Z}(p)}\right] \qquad \text{(A-7)}$$

An appropriate set of boundary and initial conditions are:

1. Constant terminal pressure case with external boundary pressure constant

INITIAL CONDITION

$$p(x, o) = p_i$$

BOUNDARY CONDITIONS

$$p\ (o, t) = p_w$$

$$p\ (L, t) = p_i$$

2. Constant terminal pressure case with external boundary sealed

INITIAL CONDITION

$$p(x,o) = p_i$$

BOUNDARY CONDITIONS

$$p(o,t) = p_w$$

$$\frac{\partial p}{\partial x} \quad (L,t) = o$$

APPENDIX B

DISCRETIZATION OF PARTIAL

DIFFERENTIAL EQUATION AND METHOD OF SOLUTION

DISCRETIZATION OF PARTIAL DIFFERENTIAL EQUATION AND METHOD OF SOLUTION

CRANK-NICHOLSON IMPLICIT-ONE DIMENSION

From Appendix A, the diffusivity equation for flow of a real gas is:

$$\frac{\partial}{\partial x}\left[W(p)\,K(x)\,\frac{\partial p^2}{\partial x}\right] = \frac{\phi}{\bar{p}}\,\frac{\partial}{\partial t}\left[\frac{p^2}{z(p)}\right] \qquad \text{(B-1)}$$

Differentiating Equation (B-1) gives:

$$K(x)\,\frac{\partial p^2}{\partial x}\,\frac{\partial W(p)}{\partial x} + W(p)\,K(x)\,\frac{\partial^2 p^2}{\partial x^2} + \frac{\partial p^2}{\partial x}\,W(p)\,\frac{\partial K(x)}{\partial x} = \frac{\phi}{p}\,\frac{\partial}{\partial t}\left[\frac{p^2}{z(p)}\right] \qquad \text{(B-2)}$$

To formulate a difference equation for Equation (B-2) a network having mesh width of Δx and Δt is established as portrayed in Figure (B-1).

Taylor's series expansion provides the approximation to the spatial derivatives. Consider any point j on the grid spacing

$$p_{j+1,k} = p_{j,k} + \frac{\partial p^2}{\partial x}\,\Delta x + \frac{\partial^2 p^2}{\partial x^2}\,\frac{\Delta x^2}{2!} + \ldots \qquad \text{(B-3)}$$

$$p_{j-1,k} = p_{j,k} - \frac{\partial p^2}{\partial x}\,x + \frac{\partial^2 p^2}{\partial x^2}\,\frac{\Delta x^2}{2!} \ldots\ldots \qquad \text{(B-4)}$$

Subtraction of Equation (B-3) and Equation (B-4) neglecting terms of the order of $\frac{\partial^3 p}{\partial x^3}\,\frac{\Delta x^3}{3!}$ and higher gives:

$$\frac{\partial p^2}{\partial x} = \frac{p^2_{j+1,k} - p^2_{j-1,k}}{2\Delta x} \qquad \text{(B-5)}$$

The addition of Equation (B-3) and Equation (B-4) with terms of order $\frac{\partial^4 p^2}{\partial x^4} \quad \frac{\Delta x^4}{4!}$ and higher neglected yields:

$$\frac{\partial^2 p^2}{\partial x^2} = \frac{p^2_{j+1,k} - 2p^2_{j,k} + p^2_{j-1,k}}{\Delta x^2} \qquad \text{(B-6)}$$

Similarly expanding $p_{j,k+1}$ about $p_{j,k}$ and neglecting the second and higher order terms gives:

$$\frac{\partial}{\partial t}\left[\frac{p^2}{z(p)}\right] = \frac{1}{\Delta t}\left[\frac{p_{j,k+1}}{z(p_{j,k+1})} - \frac{p_{j,k}}{z(p_{j,k})}\right] \qquad \text{(B-7)}$$

This derivative will be centered at k+1/2.

Finally, the derivative $\partial K(x)/\partial x$ differs from the derivative of Equation (B-5) only in the respect that values of the property K(x) are located at $x_{j+1/2}$. Therefore the derivative approximation is

$$\frac{\partial K(x_j)}{\partial x} = \frac{\Delta K(x_j)}{\Delta x} = \frac{K(x_{j+1/2}) - K(x_{j-1/2})}{\Delta x} \qquad \text{(B-8)}$$

Equations (B-5) and (B-6) represent the finite difference approximations to the spatial derivatives.

However since it is desirable to employ Crank-Nicholson approximations, the appropriate equations are:

$$\frac{\partial p^2}{\partial x} = \frac{1}{4\,\Delta x}\left[p^2_{j+1,k} - p^2_{j-1,k} + p^2_{j+1,k+1} - p^2_{j-1,k+1}\right] \tag{B-9}$$

$$\frac{\partial^2 p^2}{\partial x^2} = \frac{1}{2\,\Delta x^2}\left[p^2_{j+1,k} - 2p^2_{j,k} + p^2_{j-1,k} + p^2_{j+1,k+1} - 2p^2_{j,k+1} + p^2_{j-1,k+1}\right] \tag{B-10}$$

The substitution of Equations (B-7), (B-8), B-9) and (B-10) into Equation (B-2), and the collection of terms according to their time and space subscripts with respect to pressure yields:

$$\left[K(x_j)\ \Delta W(p_j) + 2W(p_j)\ \Delta K(x_j) + 4W(p_j)\ K(x_j)\right]\ p^2_{j+1,k}$$

$$+\left[\frac{8\phi\,\Delta x^2}{\bar{p}\ \Delta t\ z(p_j)} - 8W(p_j)\ K(x_j)\right]\ p^2_{j,k} + \left[K(x_j)\ \Delta W(p_j) - 2W(p_j)\ \Delta K(x_j) + 4W(p_j)K(x_j)\right]$$

$$p^2_{j+1,k} = \left[-K(x_j)\ \Delta W(p_j) - 2W(p_j)\ \Delta K(x_j) - 4W(p_j)\ K(x_j)\right]\ p^2_{j+1,k+1}$$

$$+\left[\frac{8\phi\,\Delta x^2}{\bar{p}\ \Delta t\ x(p_j)} + 8W(p_j)\ K(x_j)\right]\ p^2_{j,k+1} + \left[K(x_j)\ \Delta W(p_j) + 2W(p_j)\ \Delta K(x_j) - 4W(p_j)K(x_j)\right]$$

$$p^2_{j-1,k+1} \tag{B-11}$$

wherein

$$\Delta K(x_j) = K(x_{j+1/2}) - K(x_{j-1/2})$$

$$\Delta W(p_j) = W(p_{j+1}) - W(p_{j-1})$$

SOLUTION OF THE NON-LINEAR C-N IMPLICIT EQUATION

The C-N implicit procedure in one-dimension as illustrated in Figure (B-1) was applied utilizing Equation B-11 with appropriate initial and boundary conditions to obtain the pressure distribution for each time step.

For convenience Equation (B-11) is written as :

$$A(p^2_{j-1,k+1}) + B(p^2_{j,k+1}) + C(p^2_{j+1,k+1}) = D_{j,k} \qquad (B-12)$$

wherein:

$$A = K(x_j)\Delta W(p_j) + 2W(p_j)\Delta K(x_j) - 4W(p_j)K(x_j)$$

$$B = \frac{8\phi\Delta x^2}{\bar{p}\Delta t\, z(p_j)} + 8W(p_j)\,K(x_j)$$

$$C = -K(x_j)\Delta W(p_j) - 2W(p_j)\Delta K(x_j) - 4W(p_j)\,K(x_j)$$

and

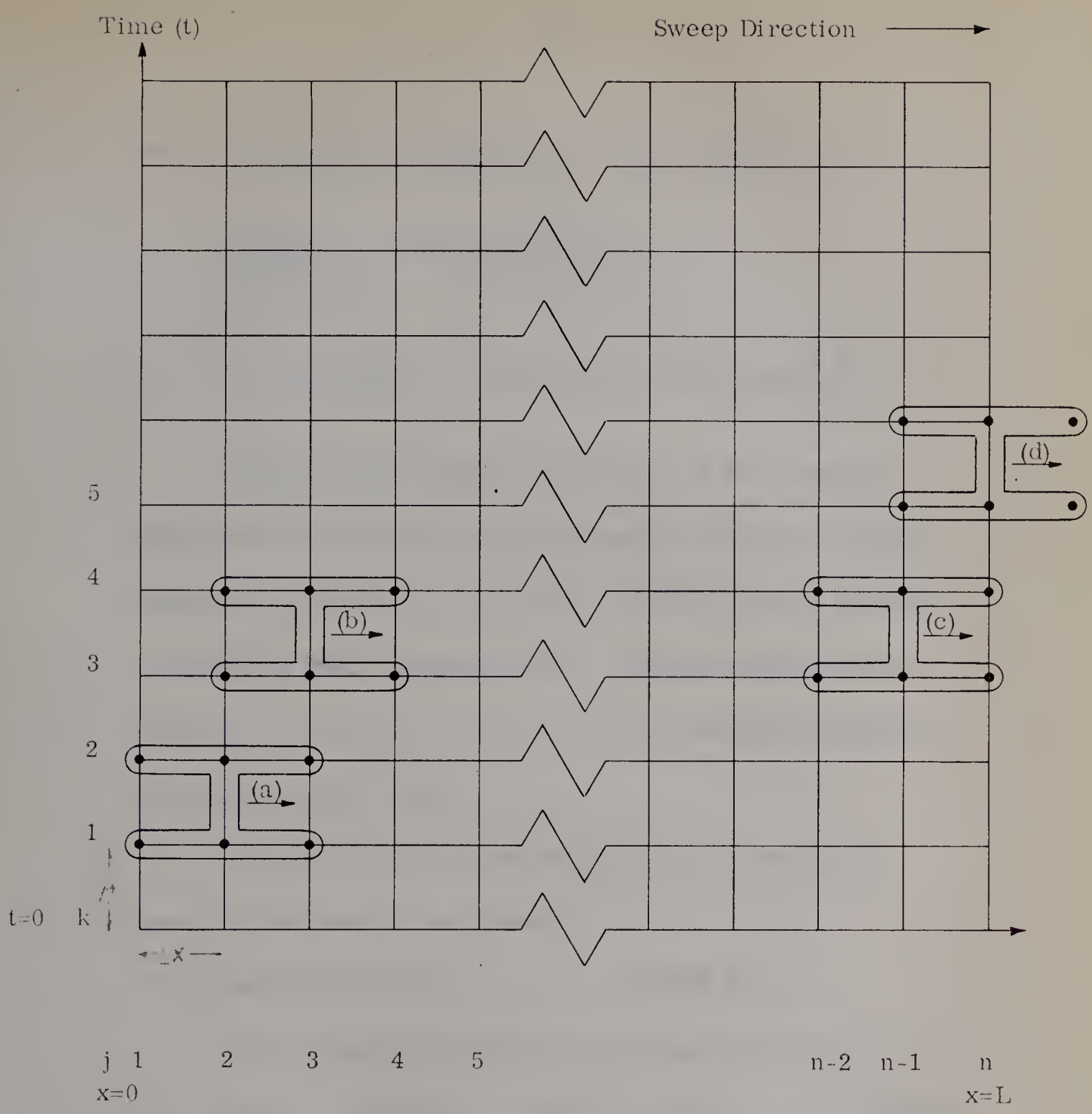

ONE DIMENSIONAL LINEAR CRANK NICHOLSON IMPLICIT PROCEDURE GRID POINTS AND TIME LEVELS

FIGURE B-1

$$D= \left[K(x_j)\Delta W(p_j) + 2W(p_j)\Delta K(x_j) + 4W(p_j)\,K(x_j)\right] p^2_{j+1,k}$$

$$+\left[\frac{8\phi\Delta x^2}{\bar{p}\,\Delta t z(p_j)} - 8W(p_j)K(x_j)\right] p^2_{j,k}$$

$$+\left[-K(x_j)\Delta W(p_j) - 2\,W(p_j)\Delta K(x_j) + 4\,W(p_j)K(x_j)\right] p^2_{j-1,k}$$

Solution of the pressure distribution at time step k+1 commenced by guessing a pressure profile at this time step to permit the evaluation of A, B and C. The steady state equation provided this initial guessed profile. Subsequent distributions employed to evaluate A, B and C represent solutions obtained in a previous iteration step.

The application of Equation (B-12) to the first set of boundary conditions is as follows:

GRID POINT (j=2) -- FIGURE (B-1-a)

At this location Equation (B-12) takes on the form:

$$(A)\, p^2_{1,k+1} + (B)\, p^2_{2,k+1} + (C)\, p^2_{3,k+1} = D_{1,k} \qquad \text{(B-13)}$$

however from boundary conditions presented in Appendix A constant terminal pressure implies

$$p^2_{1,k+1} = p^2_w$$

therefore Equation (B-13) becomes

$$(B)\ p^2_{2,k+1} + (C)\ p^2_{3,k+1} = D_{1,k} - (A)\ p^2_w \qquad (B\text{-}14)$$

where $p^2_{2,k+1}$ and $p^2_{3,k+1}$ are the only unknowns, since B and C were evaluated from the guessed profile.

INTERIOR GRID POINTS ($2<j<n-1$) -- FIGURE (B-1-b)

For all interior grid points Equation (B-12) becomes:

$$(A)\ p^2_{j-1,k+1} + (B)p^2_{j,k+1} + (C)\ p^2_{j+1,k+1} = D_{j,k} \qquad (B\text{-}15)$$

where $p^2_{j+1,k+1}$, $p^2_{j,k+1}$ and $p^2_{j-1,k+1}$ are unknowns

GRID POINT ($j=n-1$) -- FIGURE (B-1-c)

The external boundary condition states

$$p^2_{n,k+1} = p^2_i$$

therefore Equation (B-12) at this location is:

$$(A)\ p^2_{n-2,k+1} + (B)\ p^2_{n-1,k+1} = (D)_{n-1,k} - (C)p^2_i \qquad (B\text{-}16)$$

The one relationship of Equation (B-14), the n-2 relationships of Equation (B-15) and the one relationship of Equation (B-16) provide for n conditions for evaluating improved values of $p_{j,k+1}$, $2 \leq j \leq n-1$, over those guessed. For example, if n=6, these conditions

are as represented in Table B-1

TABLE B-1

C-N IMPLICIT PROCEDURE

j	p_1	p_2	p_3	p_4	p_5	p_6	
1	B_1	C_1					$D_1 - A_1 p_w^2$
2	A_2	B_2	C_2				D_2
3		A_3	B_3	C_3			D_3
4			A_4	B_4	C_4		D_4
5				A_5	B_5	C_5	D_5
6					A_6	B_6	$D_6 - C_6 p_i^2$

or in matrix notation

$$[A]\ \vec{p} = \vec{b} \qquad \text{(B-17)}$$

Solutions of the pressure vector $\vec{p}$ was obtained by matrix inversion utilizing the square-root algorithm modified for non-symmetric matrices. Hence

$$\vec{p} = [A^{-1}]\ \vec{b}$$

Evaluating the second set of boundary conditions involving the sealed boundary required altering only two of the n equations. The boundary condition implies:

$$\frac{\partial p^2_{n,k+1}}{\partial x} = o$$

which can be incorporated into Equation (B-13) by setting

$$p^2_{n+1,k+1} = p^2_{n-1,k+1} \qquad \text{(B-21)}$$

Interior grid points, to which Equation (B-15) applies now extend over the interval $2<j<n$ and at:

GRID POINT ($j = n$) -- FIGURE (B-1-d)

Introducing the external boundary condition as stated by Equation (B-21) to Equation (B-13) yields

$$(A+C)\, p^2_{n-1,\ k+1} + (B)\, p^2_{n,\,k+1} = (D)_{n,\,k} \qquad \text{(B-22)}$$

From this stage on the solution of the pressure profiles is identical to that employed in solving the first set of boundary conditions.

Because the partial differential equation describing gas flow is non-linear, it is necessary to iterate at each time step. If r indicates the rth iteration, a solution for $\vec{p}$ was considered to be obtained when:

$$\left| \frac{p^{(r+1)} - p^{(r)}}{p^{(r+1)}} \right| < \epsilon$$

Where ϵ represents the maximum permissive difference between pressures of successive iterations. In this investigation ϵ was set equal to 2×10^{-3} so that the difference between the accepted pressure and the pressure at the previous iteration was less than 0.1 pounds per square inch.

APPENDIX C

COMPUTER PROGRAM

COMPUTER PROGRAM

The computer program, which was written to solve the unsteady state gas flow problem for the set of boundary conditions of constant terminal pressure with constant pressure at the external boundary, may be divided into six parts.

(1) MAIN PROGRAM - The main program computes the pressure distribution in a linear heterogeneous system by solving the continuity-Darcy flow equations for gas. A Crank-Nicholson implicit procedure is employed along with a Function iterative technique.

(2) PRESSURE COEFFICIENT SUBROUTINE - The elements of the matrix at time k+1 and the elements of the vector corresponding to the known pressure distribution are calculated by this subroutine as requested by the main program.

(3) COMPRESSIBILITY SUBROUTINE - Utilizing Lagrangian iterpolation and correlations of Helsenrath et al [16], this subroutine provides the subroutine discussed in Part (2) with compressibility of nitrogen gas as a function of pressure and temperature.

(4) VISCOSITY SUBROUTINE - This subroutine employs a correlation proposed by Kestin et al [19] to calculate the

viscosity of nitrogen gas for SUBROUTINE PRCOEFF.

(5) EFFECTIVE PERMEABILITY SUBROUTINE - The variation of permeability with distance is provided by this subroutine for the subroutine discussed in Part (2).

(6) SQUARE-ROOT MATRIX INVERSION SUBROUTINE - This subroutine inverts the matrix developed by the subroutine whose function was described in Part (2). In matrix notation the equation describing unsteady state gas flow at every grid point takes on the following form,

$$[A]\vec{p} = \vec{b}$$

Firstly the subroutine inverts the matrix [A],

$$[A]^{-1}[A]\vec{p} = [A]^{-1}\vec{b}$$

and then solves for the vector $\vec{p}$

or $$[I]\vec{p} = [A]^{-1}\vec{b}$$

$$\vec{p} = [A]^{-1}\vec{b}$$

which represents the unknown pressure distribution at time k+1.

To solve the second set of boundary conditions the main program must be modified by altering the equation which evaluates the vector $\vec{b}$. The only contribution to this

vector from the boundary conditions will be from the constant terminal pressure boundary. Furthermore, to SUBROUTINE PRCOEF must be added an equation which evaluates the element at the $(n+1)\Delta x$ position. These alterations are also explained in Appendix B.

COMPUTER PROGRAM NOMENCLATURE

The following list contains those quantities which are pertinent to the understanding of the program.

A	matrix of non-linear terms at $(i+1)_{\Delta}t$
A A	elements of [A] at the boundaries
ALIP	Lagrangian interpolation polynomial
B) C) D)	coefficients of equation describing compressibility factor
BA	vector of known quantities at time $(i)_{\Delta}t$
BBB	slip coefficient
BC	matrix at time $(i)_{\Delta}t$
DELT	time increment
DELTEC	temperature differential for viscosity correction
DELWPS	differential of WPS from one grid point to the next
DELXSQ	distance increment squared
DIFP	factional difference between pressures for two sequential iterations
DP DPRESS	dimensional pressure
DT	dimensionless time
DX	dimensionless distance

EFFK	effective permeability at grid point
IA	number of time steps
IG	number of sets of B, C, D
II	permeability flag
JA	number of grid points at any time interval
JJ	matrix flag
LA	number of data sets
LK) I)	time step
LL	number of rows and columns in matrix [A]
P) PA)	pressure
PERM	liquid permeability of distance increment
PERML	liquid permeability of core sample
PHI	porosity
PJ1) PJ2) PJPI1) PJPI2) PJPI3)	components of elements making up matrix
PM	mean pressure
PN) PX)	iterated pressure evaluated for time $(i+1)\Delta t$

PNSQ	PN squared
PO	known pressure including initial conditions
T	time
TE	temperature
TP	temperatures associated with B, C, D
URATIO	ratio of gas viscosities at P and one atmosphere
VN2	viscosity
WPRS	inverse of product of compressibility and viscosity
X	distance
Z	compressibilities corresponding to TP
ZN2	interpolated compressibility factor

The preceding nomenclature summary does not include that used in subroutine SQROOT. This subroutine was modified and utilized by Allada, and only the following must be known to use it:

A	the matrix of nonlinear terms $[A]$
BA	the known vector $\vec{b}$
M=LL	the size of the matrix $[A]$
Y	the solution vector $\vec{PNSQ}$

```
C              CONSTANT TERMINAL PRESSURE CASE
C        WITH CONSTANT PRESSURE AT THE EXTERNAL BOUNDARY
C
      DIMENSION A(20,20),BA(15),BC(20,20),DPRESS(20,20),PN(1
     15),PNSQ(15),PO(20,15),PX(15),DT(15),DP(15,15),DX(15)
      COMMON B(10),C(10),D(10),P(15),PM(15),T(15),X(15),TP(1
     10),PERM(15),BBB
      COMMON IG,JJ,JA,LL,LK
C
C         READ IN NUMBER OF DATA SETS
      READ(5,200)LA
  200 FORMAT(1X,I3)
C
C         READ IN TEMPERATURE VALUES
      READ(5,106)IG,(TP(I),I=1,IG)
  106 FORMAT(1X,I3,6F6.2)
C
C         READ IN COMPRESSIBLITY   CONSTANTS
      READ(5,101)(B(I),C(I),D(I),I=1,6)
  101 FORMAT(1X,6E10.4)
      DO 60 M=1,LA
      WRITE(6,201)M
  201 FORMAT('1CORE NO.=',I3)
C
C         READ IN BASIC ROCK PROPERTIES AND CONDTIONS
      READ(5,100) PHI,PERML,TE,IA,JA
  100 FORMAT(1X,F5.3,3X,F6.2,3X,F5.1,2(3X,I3))
      WRITE(6,115)PHI,PERML,TE,IA,JA
  115 FORMAT(' ',F5.3,3X,F6.2,3X,F5.1,2(3X,I3))
      JAM1=JA-1
      READ(5,107)(PERM(J),J=1,JAM1)
  107 FORMAT(1X,10F7.2)
      WRITE(6,107)(PERM(J),J=1,JAM1)
      READ(5,108)BBB
  108 FORMAT(1X,F7.3)
      WRITE(6,108)BBB
C
C         READ IN BOUNDARY CONDITIONS
      READ(5,102)(PO(1,J),J=1,JA)
  102 FORMAT(1X,7F10.3)
      WRITE(6,102)(PO(1,J),J=1,JA)
      READ(5,103)(PO(I,1),PO(I,JA),I=2,IA)
  103 FORMAT(1X,7F10.3)
      WRITE(6,103)(PO(I,1),PO(I,JA),I=2,IA)
C
C         READ IN TIME VALUES
      READ(5,104)(T(I),I=1,IA)
  104 FORMAT(1X,11F7.3)
      WRITE(6,104)(T(I),I=1,IA)
C
C         READ IN DISTANCE VALUES
      READ(5,105)(X(J),J=1,JA)
  105 FORMAT(1X,13F6.2)
      WRITE(6,105)(X(J),J=1,JA)
```

```
      IAM1=IA-1
      DO 40 I=1,IAM1
      LK=I
C
C        CALCULATE COEFFICIENTS OF PRESSURES AT TIME=T+1
      DO 5 J=1,JA
    5 PN(J)=SQRT((X(J)/X(JA))*(PO(I+1,JA)*PO(I+1,JA)-PO(I+1,
     11)*PO(I+1,1))+PO(I+1,1)*PO(I+1,1))
    6 DO 7 J=1,JA
      P(J)=PN(J)
    7 PM(J)=.5*(PN(J)+PO(I,J))
      JJ=1
      CALL PRCOEF(PHI,TE,A)
C
C        CALCULATE COEFFICIENTS OF PRESSURES AT TIME=T
      DO 10 J=1,JA
   10 P(J)=PO(I,J)
      JJ=2
      CALL PRCOEF(PHI,TE,BC)
C
C        CALCULATE VECTOR OF PRESSURES AT TIME=T
      DO 15 L=2,JAM1
      BA(L)=0.0
      DO 15 J=1,JA
      A1=0.0
      IF(L.EQ.2.AND.J.EQ.1)A1=A(2,1)
      A2=0.0
      IF(L.EQ.JAM1.AND.J.EQ.JA)A2=A(JAM1,JA)
   15 BA(L)=BA(L)+BC(L,J)*P(J)*P(J)-A1*PO(I+1,1)*PO(I+1,1)-A
     12*PO(I+1,JA)*PO(I+1,JA)
      JAM2=JA-2
      LL=JAM2
      DO 16 L=1,JAM2
      DO 16 J=1,JAM2
   16 A(L,J)=A(L+1,J+1)
      DO 17 L=1,JAM2
   17 BA(L)=BA(L+1)
C
C        CALCULATE PRESSURES AT TIME=T+1
      CALL SQROOT(A,BA,PNSQ)
C
C        CHECK CONVERGENCE OF PRESSURE VALUES
      II=0
      DO 20 J=2,JAM1
      PX(J)=SQRT(PNSQ(J-1))
      DIFP=ABS((PX(J)-PN(J))/PX(J))
      IF(DIFP.GT.0.002)II=1
      PN(J)=PX(J)
   20 PO(I+1,J)=PN(J)
      IF(II.EQ.1)GO TO 6
   40 CONTINUE
      WRITE(6,110)
  110 FORMAT('-PRESSURE PROFILE FOR CONSTANT PRESSURE AT E',
     1'XTERNAL BOUNDARY')
```

```
      DO 45 I=1,IA
   45 WRITE(6,111)T(I),(PO(I,J),J=1,JA)
  111 FORMAT(' ',F7.3,2X,13(1X,F6.2))
      DO 57 I=1,IA
      DO 57 J=1,JA
      IF((PO(I,1)**2.)-(PO(I,JA)**2.))55,56,55
   55 DPRESS(I,J)=(PO(I,J)**2.-PO(I,JA)**2.)/(PO(I,1)**2.-PO
     1(I,JA)**2.)
      GO TO 57
   56 DPRESS(I,J)=0.0
   57 CONTINUE
      WRITE(6,130)
  130 FORMAT('-',20X,'DIMENSIONLESS PRESSURE PROFI',
     1'LE')
      WRITE(6,132)
  132 FORMAT('0',2X,'TIME',20X,'P(X,T)**2-PF**2/PE**2-PF**',
     1'2)
      DO 58 I=1,IA
   58 WRITE(6,131)T(I),(DPRESS(I,J),J=1,JA)
  131 FORMAT(' ',F7.3,2X,13(1X,F6.4))
      PR=PO(1,JA)
      CALL VISCN2(PR,TE,VN2)
      DO 65 I=1,IA
      DT(I)=(.633E-03*PO(1,JA)*PERML*T(I))/(PHI*VN2*X(JA)**2
     1)
      DO 65 J=1,JA
      DX(J)=X(J)/X(JA)
      DP(I,J)=PO(I,J)/PO(1,JA)
   65 CONTINUE
      WRITE(6,140)
  140 FORMAT('0',30X,'P(X,T)/PF')
      WRITE(6,141)(DX(J),J=1,JA)
  141 FORMAT(10X,13(1X,F6.4))
      WRITE(6,143)
  143 FORMAT(1X,'DTIME')
      DO 70 I=1,IA
   70 WRITE(6,142)DT(I),(DP(I,J),J=1,JA)
  142 FORMAT(' ',F7.4,2X,13(1X,F6.4))
   60 CONTINUE
      STOP
      END
```

```
      SUBROUTINE PRCOEF(PHI,TE,W)
      DIMENSION W(20,20),WPRS(3)
      COMMON B(10),C(10),D(10),P(15),PM(15),T(15),X(15),TP(1
     10),PERM(15),BBB
      COMMON IG,JJ,JA,LL,LK
      JAM1=JA-1
      DO 12 L=2,JAM1
      DO 12 J=1,JA
      IF(J.LT.L-1)GO TO 11
      IF(J.GT.L+1)GO TO 11
      IF(L.EQ.J)GO TO 7
      IF(J.GT.L)GO TO 9
      LA=L-1
      DO 2 I=1,3
      PR=P(LA)
      CALL COMPN2(PR,TE,ZN2)
      CALL VISCN2(PR,TE,VN2)
      WPRS(I)=1./(VN2*ZN2)
      LA=LA+1
    2 CONTINUE
      II=1
      CALL PERMEF(L,II,EFFK)
      DELWPS=WPRS(3)-WPRS(1)
      PJP11=EFFK*DELWPS
      PJP13=4.*WPRS(2)*EFFK
      II=2
      CALL PERMEF(L,II,EFFK)
      PJP12=WPRS(2)*EFFK*2.
      IF(JJ.EQ.2)GO TO 6
      W(L,J)=PJP11+PJP12-PJP13
      GO TO 12
    6 W(L,J)=-PJP11-PJP12+PJP13
      GO TO 12
    7 DELXSQ=X(L+1)*X(L)-X(L)*X(L)-X(L+1)*X(L-1)+X(L)*X(L-1)
      DELT=T(LK+1)-T(LK)
      PR=P(L)
      CALL COMPN2(PR,TE,ZN2)
      PJ1=.1264E+05*PHI*DELXSQ/(P(JA)*DELT*ZN2)
      PJ2=2.*PJP13
      IF(JJ.EQ.2)GO TO 8
      W(L,J)=PJ1+PJ2
      GO TO 12
    8 W(L,J)=PJ1-PJ2
      GO TO 12
    9 IF(JJ.EQ.2)GO TO 10
      W(L,J)=-(PJP11+PJP12+PJP13)
      GO TO 12
   10 W(L,J)= PJP11+PJP12+PJP13
      GO TO 12
   11 W(L,J)=0.0
   12 CONTINUE
      RETURN
      END
```

```
      SUBROUTINE COMPN2(PX,TE,ZN2)
      DIMENSION ALIP(10),Z(10)
      COMMON B(10),C(10),D(10),P(15),PM(15),T(15),X(15),TP(1
     10),PERM(15),BBB
      COMMON IG,JJ,JA,LL,LK
      PA=PX/14.696
      ZN2=0.0
      TEK=(TE-32.)*(5./9.)+273.1
      DO 15 I=1,IG
      ALIP(I)=1.0
      DO 10 J=1,IG
      IF(I.EQ.J)GO TO 10
      ALIP(I)=ALIP(I)*((TEK-TP(J))/(TP(I)-TP(J)))
   10 CONTINUE
      Z(I)=1.+B(I)*PA+C(I)*PA**2.+D(I)*PA**3.
      IF(TEK.EQ.TP(I)) GO TO 16
   15 ZN2=ZN2+ALIP(I)*Z(I)
      GO TO 17
   16 ZN2=Z(1)
   17 RETURN
      END
```

```
      SUBROUTINE VISCN2(PX,TE,VN2)
      COMMON B(10),C(10),D(10),P(15),PM(15),T(15),X(15),TP(1
     10),PERM(15),BBB
      COMMON IG,JJ,JA,LL,LK
      PA=PX/14.696
      PMC=PA-1.
      URATIO=1.+.895E-03*PMC+.612E-06*PMC**2.+3.997E-08*PMC*
     1*3.
      VISN2=URATIO*1.778E-02
      DELTEC=(TE-32.)*(5./9.)-25.
      VN2=VISN2+DELTEC*.455E-04
      RETURN
      END
```

```
      SUBROUTINE PERMEF(L,II,EFFK)
      COMMON B(10),C(10),D(10),P(15),PM(15),T(15),X(15),TP(1
     10),PERM(15),BBB
      COMMON IG,JJ,JA,LL,LK
      IF(II.EQ.2)GO TO 5
      DELX1=(X(L)-X(L-1))/2.
      DELX2=(X(L+1)-X(L))/2.
      EFFK=(DELX1*PERM(L-1)+DELX2*PERM(L))/(DELX1+DELX2)
      GO TO 10
    5 EFFK=PERM(L)-PERM(L-1)
   10 RETURN
      END
```

```
      SUBROUTINE SQROOT(A,BA,Y)
      DIMENSION A(20,20),AA(20,20),AL(20,20),AM(20,20),AU(20
     1,20),AV(20,20),BA(15),BB(15),BC(20,20),DIF(15),PCENT(1
     15),Y(15)
      COMMON B(10),C(10),D(10),P(15),PM(15),T(15),X(15),TP(1
     10),PERM(15),BBB
      COMMON IG,JJ,JA,LL,LK
  151 FORMAT(1H ,29H THE METHOD IS NOT APPLICABLE)
      M=LL
      DO 1 I=1,M
      DO 2 J=1,M
    2 AA(I,J)=A(I,J)
    1 BB(I)=BA(I)
C
C     CALCULATION OF L AND U
      DO 105 K=2,M
      KK=K-1
      DO 104 J=1,KK
      AL(J,K)=0.0
      AM(J,K)=0.0
      AU(K,J)=0.0
  104 AV(K,J)=0.0
  105 CONTINUE
      IF(A(1,1).EQ.0.) GO TO 150
  106 XIS=ABS(A(1,1))
      AL(1,1)=SQRT(XIS)
      AU(1,1)=A(1,1)/AL(1,1)
      DO 107 J=2,M
      AU(1,J)=A(1,J)/AL(1,1)
  107 AL(J,1)=A(J,1)/AU(1,1)
      DO 115 K=2,M
      KK=K-1
      VALUE=0.0
      DO 108 J=1,KK
  108 VALUE=VALUE+AL(K,J)*AU(J,K)
      ZX=A(K,K)-VALUE
      IF(ZX.EQ.0.) GO TO 150
  109 ZXX=ABS(ZX)
      AL(K,K)=SQRT(ZXX)
      AU(K,K)=ZX/AL(K,K)
      KP=K+1
      KK=K-1
      IF(KP.GT.M ) GO TO 115
      DO 112 I=KP,M
      ZV=0.0
      ZW=0.0
      DO 110 LP=1,KK
      ZV=ZV+AL(K,LP)*AU(LP,I)
  110 ZW=ZW+AL(I,LP)*AU(LP,K)
      AU(K,I)=(A(K,I)-ZV)/AL(K,K)
  112 AL(I,K)=(A(I,K)-ZW)/AU(K,K)
  115 CONTINUE
C
C     L AND U ARE CALCULATED
```

```
C       PROCEEDING TO CALCULATE L-INVERSE AND U-INVERSE
        DO 119 K=1,M
        AM(K,K)=1.0/AL(K,K)
  119   AV(K,K)=1.0/AU(K,K)
        DO 125 K=2,M
        KK=K-1
        DO 122 J=1,KK
        ZQ=0.0
        DO 120 L=J,KK
  120   ZQ=ZQ+AL(K,L)*AM(L,J)
  122   AM(K,J)=-ZQ/AL(K,K)
  125   CONTINUE
        IJN=M+1
        DO 135 KL=1,IJN
        K=IJN-KL
        IF(K.LE.1) GO TO 136
  126   DO 130 JK=1,K
        J=K-JK
        IF(J.LT.1) GO TO 135
  127   ZR=0.0
        JP=J+1
        DO 128 L=JP,K
  128   ZR=ZR+AU(J,L)*AV(L,K)
  130   AV(J,K)=-ZR/AU(J,J)
  135   CONTINUE
C
C       PROCEEDING TO CALCULATE G-INVERSE=U-INVERSE*L-INVERSE
  136   DO 140 K=1,M
        DO 140 J=1,M
        A(J,K)=0.0
        DO 137 L=1,M
  137   A(J,K)=A(J,K)+AV(J,L)*AM(L,K)
  140   CONTINUE
        GO TO 152
  150   WRITE(6,151)
  152   CONTINUE
        DO 153 I=1,M
        Y(I)=0.
        DO 153 J=1,M
  153   Y(I)=Y(I)+A(I,J)*BA(J)
        DO 9 J=1,M
        BOB=0.
        DO 12 I=1,M
   12   BOB=BOB+AA(J,I)*Y(I)
        DIF(J)=BB(J)-BOB
        PCENT(J)=DIF(J)*100./BB(J)
    9   CONTINUE
  202   RETURN
        END
```

APPENDIX D

GRAPHICAL RESULTS

FIGURE D-1
PRESSURE DISTRIBUTION
BEREA 1: CONSTANT TERMINAL PRESSURE WITH
CONSTANT PRESSURE AT EXTERNAL BOUNDARY

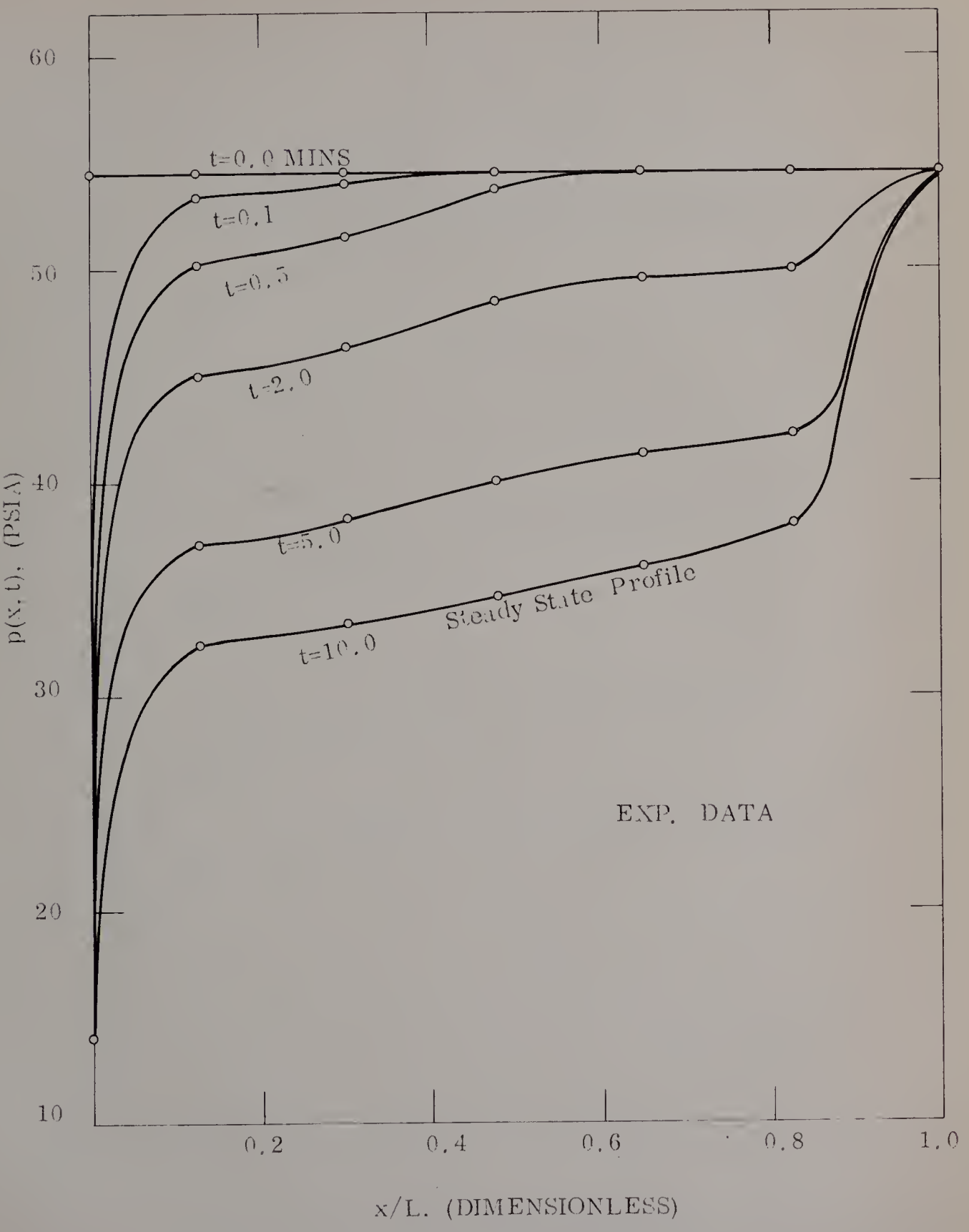

FIGURE D-2
PRESSURE DISTRIBUTION
BEREA 1: CONSTANT TERMINAL PRESSURE
WITH SEALED EXTERNAL BOUNDARY

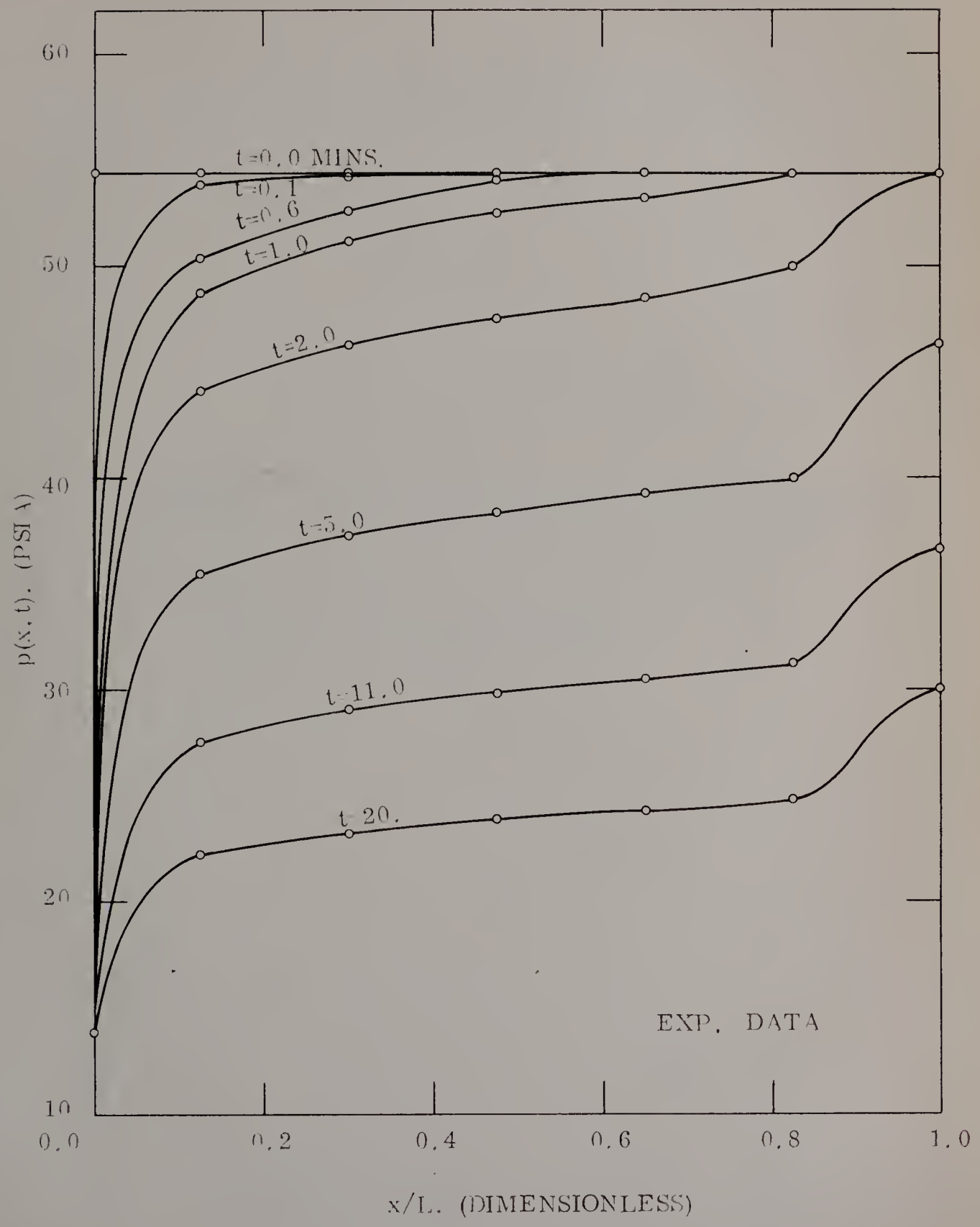

FIGURE D-3
PRESSURE DISTRIBUTION
BEREA 1A: CONSTANT TERMINAL PRESSURE WITH
CONSTANT PRESSURE AT EXTERNAL BOUNDARY

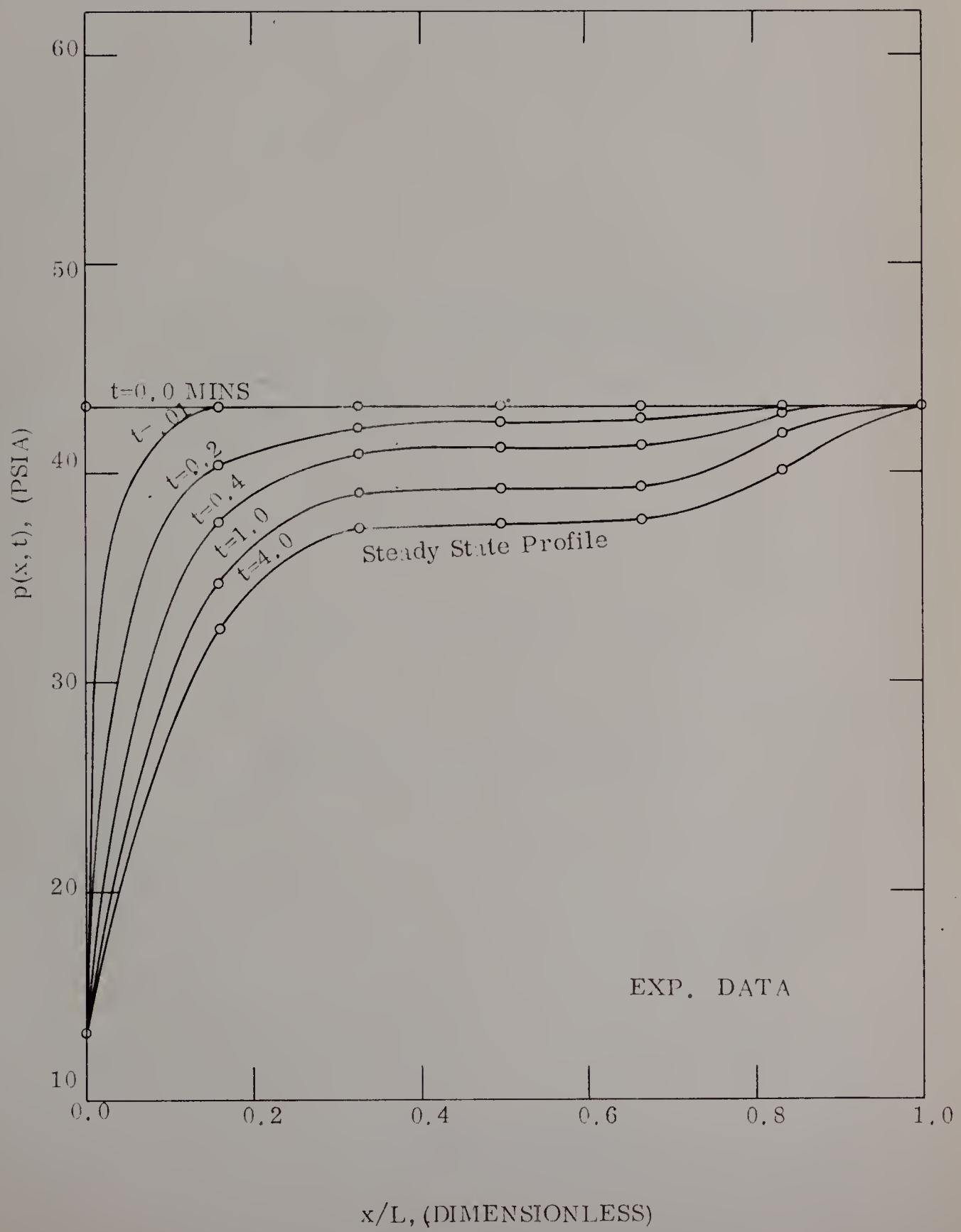

FIGURE D-4
PRESSURE DISTRIBUTION
BEREA 1A: CONSTANT TERMINAL PRESSURE WITH
SEALED EXTERNAL BOUNDARY

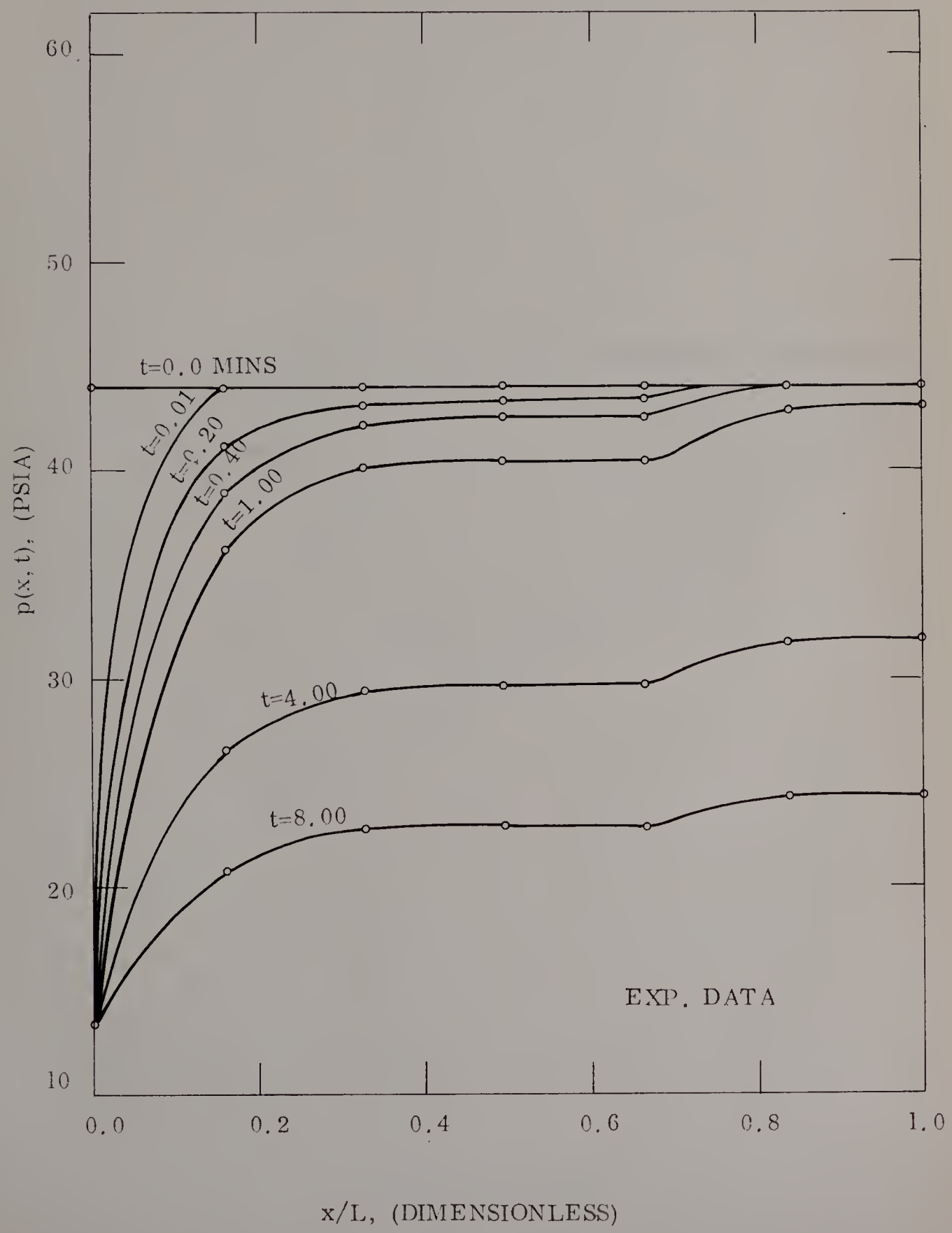

FIGURE D-5
PRESSURE DISTRIBUTION
BEREA 2: CONSTANT TERMINAL PRESSURE WITH
CONSTANT PRESSURE AT EXTERNAL BOUNDARY

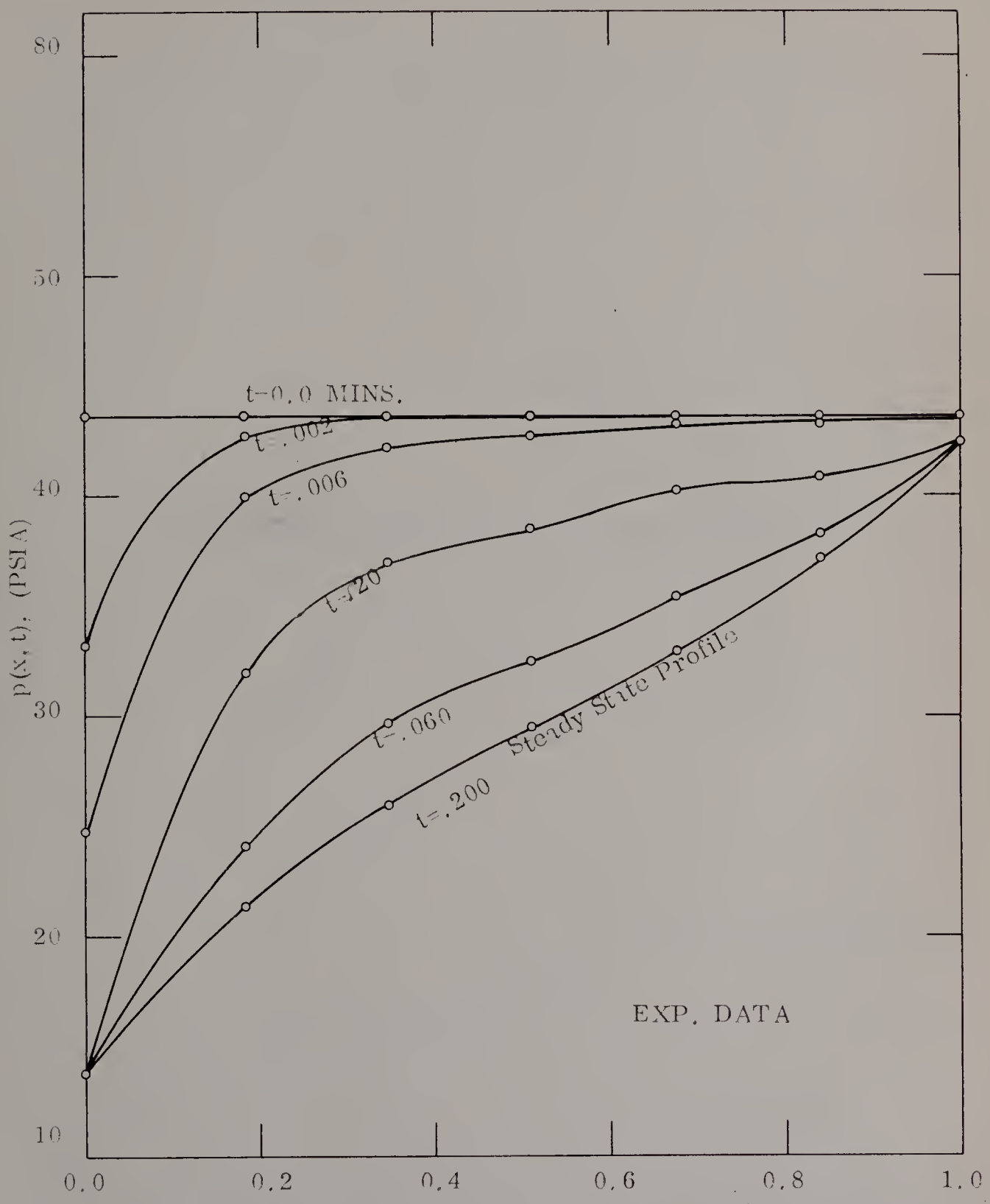

FIGURE D 6
PRESSURE DISTRIBUTION
BEREA 2: CONSTANT TERMINAL PRESSURE WITH
SEALED EXTERNAL BOUNDARY

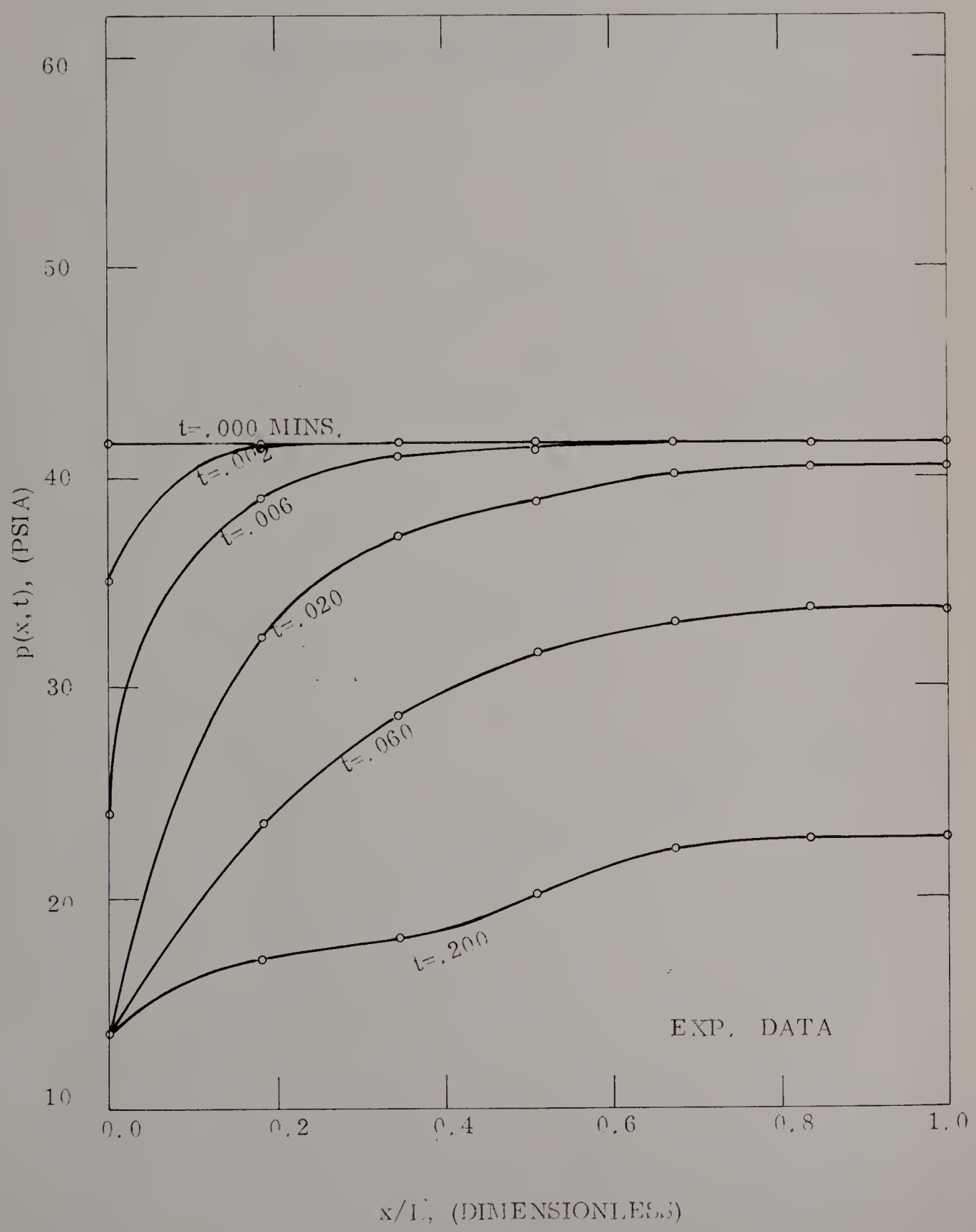

FIGURE D-7
PRESSURE DISTRIBUTION
SERIES CORE: ALUNDUM-BEREA
CONSTANT TERMINAL PRESSURE WITH SEALED
EXTERNAL BOUNDARY

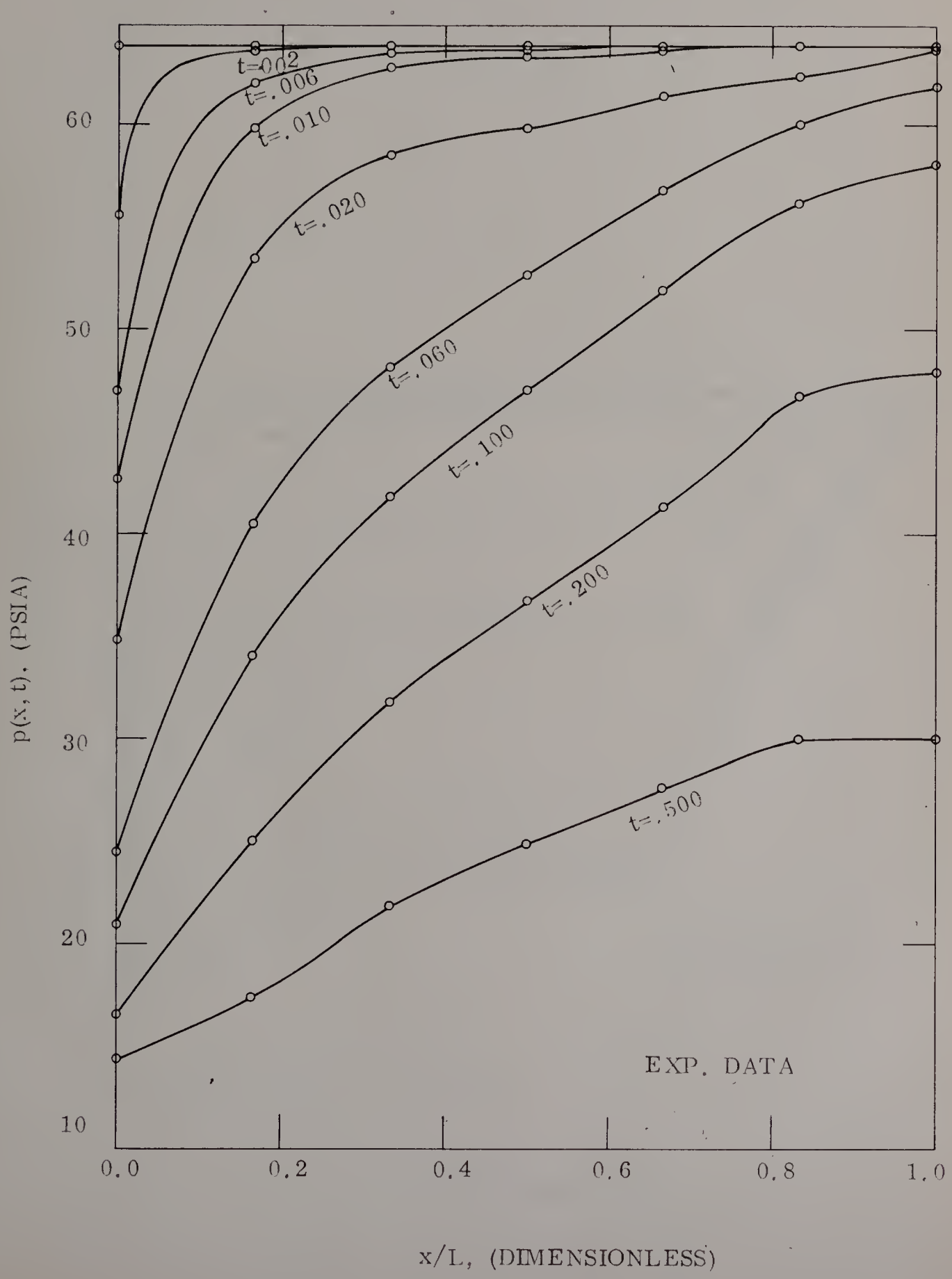

FIGURE D-8
PRESSURE DISTRIBUTION
LIMESTONE CONSTANT TERMINAL PRESSURE WITH
CONSTANT PRESSURE AT EXTERNAL BOUNDARY

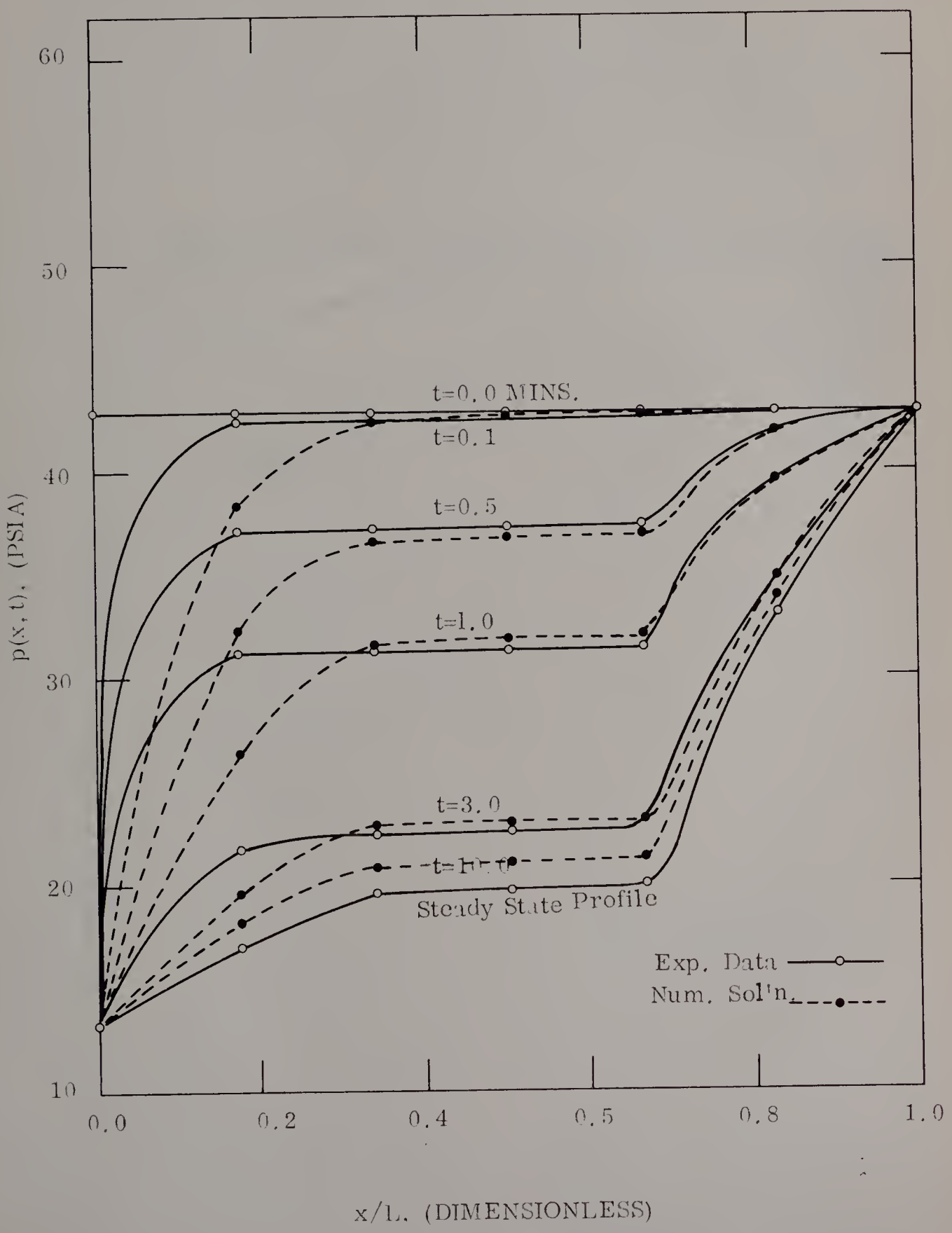

FIGURE D-9
PRESSURE DISTRIBUTION
BEREA 1: CONSTANT TERMINAL PRESSURE WITH
CONSTANT PRESSURE AT EXTERNAL BOUNDARY

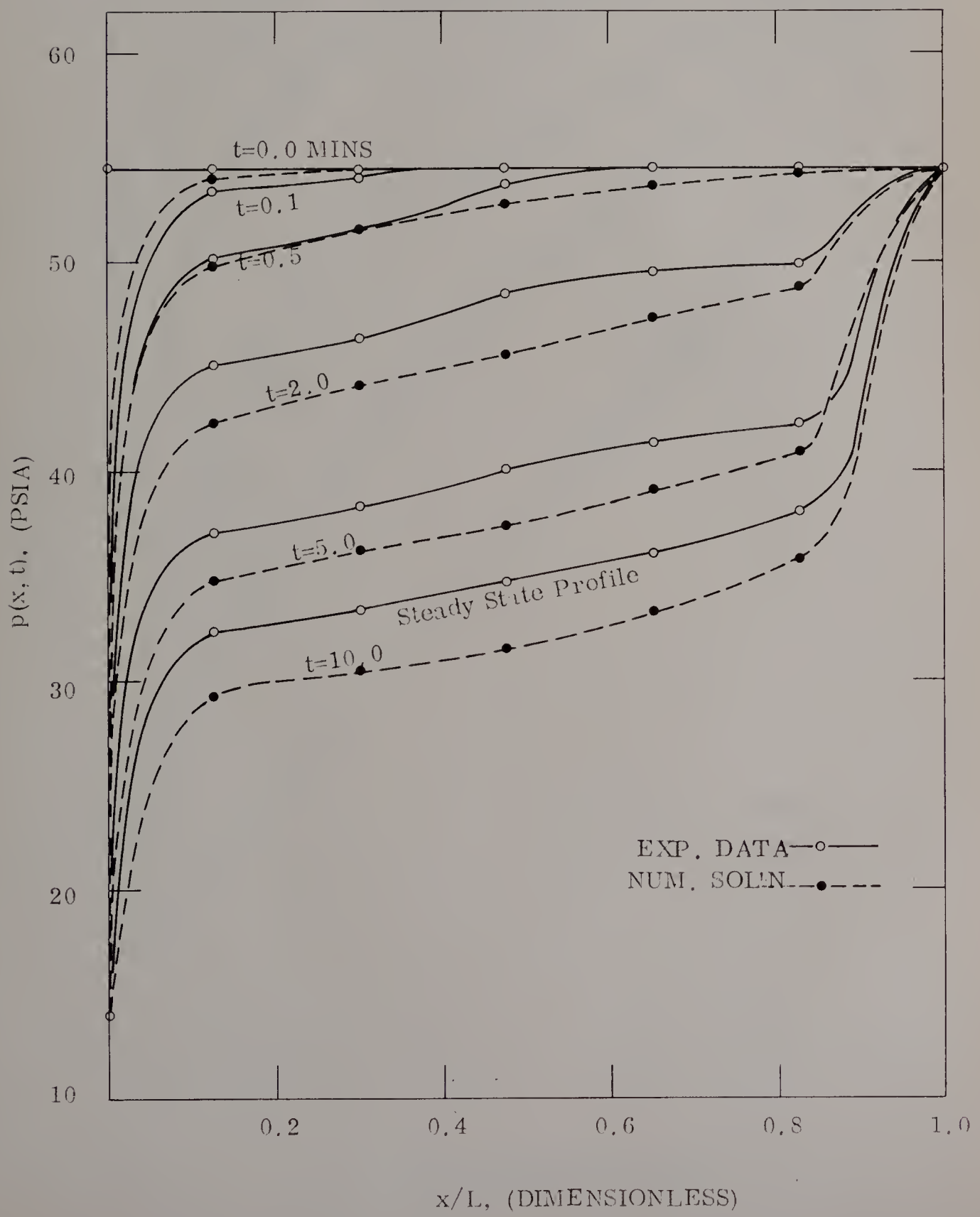

FIGURE D-10
PRESSURE DISTRIBUTION
SERIES CORE: ALUNDUM BEREA
CONSTANT TERMINAL PRESSURE WITH CONSTANT
PRESSURE AT EXTERNAL BOUNDARY